Time Domain Channel Estimation and Equalization of CP-OTFS Under Multiple Fractional Dopplers and Residual Synchronization Errors

SUVRA SEKHAR DAS[ID][1]**, (Member, IEEE), VIVEK RANGAMGARI**[ID][1]**,**
SHASHANK TIWARI[ID][1]**, (Member, IEEE), AND**
SUBHAS CHANDRA MONDAL[2]**, (Senior Member, IEEE)**
[1]G. S. Sanyal School of Telecommunications, IIT Kharagpur, Kharagpur 721302, India
[2]Wipro Ltd., Bengaluru 560035, India

Corresponding author: Suvra Sekhar Das (suvra@gssst.iitkgp.ac.in)

ABSTRACT In the last few years, orthogonal time frequency space (OTFS) modulation has received significant attention as an alternative to OFDM especially for high mobilty scenarios. In this work, we develop a delay-Doppler domain embedded pilot based time domain channel estimation for cyclic prefix (CP)-OTFS in the presence of residual frame timing offset, carrier frequency offset and fractional multiple Doppler. One of the reasons for time domain processing is that the time domain channel representation is relatively more sparse as compared to its delay Doppler domain representation in the presence of residual synchronization errors. We also describe a time domain low complexity linear minimum mean square error (MMSE) equalization and successive interference cancellation (SIC) receiver for LDPC (low density parity check) coded CP-OTFS in this work. We further show the impact of residual frame timing offset, carrier frequency offset and fractional multiple Doppler on OTFS symbols. It is seen from the extensive Monte Carlo simulation results that the estimation and compensation methods presented here provide necessary resilience properties to OTFS. We bring out the tolerance of OTFS to such residual synchronization errors. It is further observed that the SIC is able to improve the performance of the system such that it almost matches that of the ideal knowledge based MMSE equalization. We also show the performance of RCP (reduced CP)-OTFS when used with the developed channel estimation and equalization algorithms. A unified signal processing flow for OTFS and orthogonal frequency division multiplexing (OFDM) is also described in this work to motivate studies on coexistence between the two as well as to encourage investigations on a seamless transition between OFDM and OTFS based systems for future adaptive air interface design.

INDEX TERMS Channel estimation, CFO, carrier frequency offset, equalization, ICI, MMSE, OFDM, orthogonal time frequency space modulation, OTFS, SIC, successive interference cancellation, Doppler.

I. INTRODUCTION

IMT-2020 [1], [2], aka 5G, aims to provide high spectral efficiency and high reliability in high mobility scenarios, where the wireless link becomes a highly time varying multipath channel (TVMC) [3], [4]. The modified avatar of orthogonal frequency division multiplexing (OFDM), namely

The associate editor coordinating the review of this manuscript and approving it for publication was Ananya Sen Gupta[ID].

OFDM numerology [5] is the fundamental physical layer signalling technique used in 5G-New radio (5G-NR) to address this operating requirement. OFDM numerology is essentially variable subcarrier bandwidth [6] along with variable guard interval [7] as described in [8]. Such modifications not only improve the immunity of OFDM to inter-carrier interference (ICI), which is caused by high Doppler in high mobility conditions and phase noise at high carrier frequencies, but also allow a smooth transition from 4G (IMT-Advanced [9])

to 5G with minimal changes. In a recent work by the authors [10], it is shown that orthogonal time frequency space (OTFS) [11]–[13] outperforms adaptive OFDM used in 5G-NR in such high ICI conditions.

In OTFS, symbols from complex constellation are placed in the delay-Doppler grid. The signal in delay Doppler domain is converted to frequency-time domain signal by inverse symplectic finite Fourier transform (ISFFT). This frequency-time domain signal is then converted to time domain by applying inverse fast Fourier transform (IFFT) along the frequency axis for each time bin. The last part can also be identified as OFDM modulation. In situations when one cyclic prefix (CP) is added before the entire block of OFDM symbols then a reduced CP-OTFS, namely RCP-OTFS [14] signal is generated. Whereas, when a CP is added before each OFDM symbol [13], then CP-OTFS signal is created. This work is mainly focused on CP-OTFS, however a result on RCP-OTFS is also included.

Although OTFS is an orthogonal modulation scheme, yet when the signal passes through a TVMC, the received delay-Doppler domain signal encounters inter symbol interference. To demodulate the interference affected signal, receiver designs have been proposed in the literature which include linear equalizers [15], [16] and non-linear equalizers [17]–[20]. The works [18] and [19] describes a belief propagation receiver for OTFS. In [17] Markov chain Monte Carlo sampling based on the low-complexity OTFS signal detection scheme is presented. The work [16] describes localized search based non-linear receiver for rectangular pulse shaped OTFS. These receivers have a non-linear signal decoding structure and result in very high complexity. The work [16] also presents a linear receiver architecture however it is limited because it considers ideal pulse shape and hence is not practical. In [15] a low complexity linear receiver for rectangular orthogonal pulse shaped OTFS system is described. Most of the articles mentioned above assume the availability of ideal channel estimates for demodulation of the delay-Doppler OTFS data symbols.

Channel estimation being an important element of signal demodulation, a delay-Doppler domain channel estimation algorithm is described in [14]. Authors of [17] also presents a delay-Doppler domain channel estimation. Channel estimation in delay-Doppler-angle dimension for OTFS-MIMO is shown in [21]. Some initial ideas about time domain channel estimation is presented in [22]. The channel estimation and equalization for OTFS, described in the above-cited works, considers ideal synchronization conditions. To the best of the authors' knowledge there is hardly any literature available on the synchronization aspects of OTFS. In this article we consider the above-mentioned aspects in receiver design. To do so we first develop system model considering residual synchronization errors which is further used to construct channel estimation and equalization methods. The contribution in this article are summarized below.

- We describe the complete system model of CP-OTFS including the effects of residual frame timing

offset (FTO) and residual carrier frequency offset (CFO) on CP-OTFS, considering that training sequence [23] based initial synchronization is already achieved, which is not available in literature to the best of the authors' knowledge. We establish that the integer FTO and integer CFO create a cyclic shift in delay and Doppler dimensions respectively, thus introducing interference in the received delay-Doppler signal (Section III). The interference gets further enhanced with fractional CFO.

- The expression of an equivalent channel matrix in time-domain, which includes the combined effect of the TVMC, FTO, and CFO is presented in Section IV.

- We show that the structure of time domain equivalent channel matrix is invariant to Doppler values. We also demonstrate that the time domain channel matrix is more sparse than delay-Doppler domain channel matrix in the presence of fractional Doppler in Section IV-A. This makes time domain channel estimation and equalization more attractive than the delay-Doppler domain processing as in earlier reported works on channel estimation and equalization.

- We present the method for estimating time domain equivalent channel matrix in Section V, which is necessary for equalization of received signal. Unlike earlier methods which describe delay-Doppler domain channel estimation for OTFS, our channel estimation which uses energy thresholding and spline based interpolation, and equalization performed in time domain is invariant to synchronization errors. The results bring out the tolerance of OTFS to such synchronization errors.

- The time-domain channel estimation and equalization described here not only includes compensation for synchronization errors but also provides an opportunity to develop a unified representation framework for OTFS and OFDM, which helps in paving the path for a flexible reconfigurable air interface for future air interface design.

- A low complexity LMMSE based time-domain channel equalization as well as a successive interference cancellation (SIC) algorithm, which can cancel the interference emanating from the channel as well as synchronization errors, is described in Section VI and VII respectively.

Notations: We use the following notations throughout the paper. We consider $\mathbf{x}$, $\mathbf{X}$ and x to be vectors, matrices and scalars respectively. Complex conjugate value of x is given by $\bar{x}$ whereas $j = \sqrt{-1}$. We denote the set of integers between a and b Integers by $\mathbb{Z}[a\ b]$. For brevity, $a \mod M$ is represented by $[a]_M$. Expectation, Ceil, and Kronecker product operation is denoted by $E\{-\}$, $\lceil - \rceil$, and $\otimes$ respectively. Matrices $\mathbf{0}_{N \times L}$, $\mathbf{I}_N$ and $\mathbf{W}_L$ are zero matrix of size $N \times L$, identity matrix with order N and L-order normalized inverse discrete Fourier transform (IDFT) matrix respectively. The superscripts $(-)^{\mathrm{T}}$ and $(-)^{\dagger}$ denote transpose and conjugate transpose operators, respectively. The operator diag$\{\mathbf{x}\}$ generates a diagonal matrix with the diagonal entries of the

vector **x**. Circulant matrix is represented by $circ\{\mathbf{x}\}$ whose first column is **x**. The operator $vec\{\mathbf{X}\}$ denotes Column-wise vectorization of matrix $(\mathbf{X})$.

II. SYSTEM MODEL

We consider a CP-OTFS system with M sub-carriers, each of Δf Hz bandwidth, N symbols of duration $T_u = \frac{1}{\Delta f}$ sec. each with T_{CP} sec. long CP. The system has bandwidth $B = M\Delta f$ Hz. and total frame duration $T_f = NT$ sec., where $T = T_u + T_{CP}$.

A. TRANSMITTER

QAM modulated data symbols, $d(k, l) \in \mathbb{C}$, $k \in \mathbb{Z}[0 \; N-1]$, $l \in \mathbb{Z}[0 \; M-1]$, are arranged over Doppler-delay lattice $\Lambda = \{(\frac{k}{NT_u}, \frac{l}{M\Delta f})\}$. We assume that $E[d(k, l)\bar{d}(k', l')] = \sigma_d^2 \delta(k - k', l - l')$, where δ is Dirac delta function. Doppler-delay domain data $d(k, l)$ is mapped to time-frequency domain data $X(m, n)$ on lattice $\Lambda^{\perp} = \{(m\Delta f, nT)\}$, $m \in \mathbb{Z}[0 \; M-1]$ and $n \in \mathbb{Z}[0 \; N-1]$ by using inverse symplectic finite Fourier transform (ISFFT). Following [3], [24], $X(m, n)$ is expressed as,

$$X(m, n) = \frac{1}{\sqrt{NM}} \sum_{k=0}^{N-1} \sum_{l=0}^{M-1} d(k, l) e^{j2\pi[\frac{nk}{N} - \frac{ml}{M}]}. \quad (1)$$

$X(m, n)$ is converted to a time domain signal $s'(t)$ through a Heisenberg transform as,

$$s'(t) = \frac{1}{\sqrt{M}} \sum_{n=0}^{N-1} \sum_{m=0}^{M-1} X(m, n) g(t - nT_u) e^{j2\pi m\Delta f(t - nT_u)}, \quad (2)$$

After appending CP to the baseband signal $s'(t)$ we get,

$$s(t) = \frac{1}{\sqrt{M}} \sum_{n=0}^{N-1} \sum_{m=0}^{M-1} X(m, n) g(t - nT) e^{j2\pi m\Delta f(t - T_{CP} - nT)}, \quad (3)$$

where, $g(t)$ is transmitter pulse of duration T. In this work, we use rectangular pulse i.e. $g(t) = 1$ if $0 \le t \le T$ and $g(t) = 0$, otherwise. The baseband signal $s(t)$ is up-converted to the RF carrier frequency f_c to obtain the RF signal $s_{RF}(t) = s(t)e^{j2\pi f_c t}$.

We consider a baseband time varying channel with P paths having h_p complex attenuation, τ_p delay and ν_p Doppler values for the pth path where $p \in \mathbb{Z}[1 \; P]$. The delay-Doppler channel spreading function is written as,

$$h(\tau, \nu) = \sum_{p=1}^{P} h_p \delta(\tau - \tau_p) \delta(\nu - \nu_p). \quad (4)$$

The delay and Doppler values for p^{th} path is given as $\tau_p = \frac{l_p}{M\Delta f}$ and $\nu_p = \frac{k_p}{NT}$ where l_p and k_p are delay and Doppler bin number on Doppler-delay lattice Λ for p^{th} path. Let τ_{max} and ν_{max} be the maximum delay and Doppler spread. Then, channel delay length becomes $l_\tau = \lceil \tau_{max} M\Delta f \rceil$ and channel Doppler length becomes $k_\nu = \lceil \nu_{max} NT \rceil$.

The RF equivalent channel can be given as, $h_{RF}(\tau, \nu) = h(\tau, \nu)e^{j2\pi f_c \tau}$.

The received signal can be written as, $r_{RF}(t) = \int_{\tau=0}^{\tau_{max}} \int_{\nu=-\nu_{max}}^{\nu_{max}} \left(h_{RF}(\tau, \nu) s_{RF}(t - \tau) e^{j2\pi \nu(t-\tau)} \right) d\nu d\tau + \nu_{RF}(t)$, where $\nu_{RF}(t)$ is Gaussian noise with variance σ_ν^2. Therefore, $r_{RF}(t) = \sum_{p=1}^{P} \left(h_p e^{j2\pi f_c \tau_p} s(t - \tau_p) e^{j2\pi f_c(t-\tau_p)} e^{j2\pi \nu_p(t-\tau_p)} \right) + \nu_{RF}(t)$. The received signal after downconversion to base band is $r(t) = r_{RF}(t)e^{-j2\pi f_c' t}$, where $f_c' = f_c - \delta f_c$ is the receiver carrier frequency with offset δf_c. The signal $r(t)$ is,

$$r(t) = \sum_{p=1}^{P} h_p e^{j2\pi \delta f_c \tau_p} s(t - \tau_p) e^{j2\pi(\delta f_c + \nu_p)(t - \tau_p)}. \quad (5)$$

The signal $r(t)$ sampled at $Fs = B = 1/T_s = (M+L)/T$, where $L = \lceil T_{CP}B \rceil$ is the length of sampled CP and $T = T_u + T_{CP} = (M + L)T_s$, becomes,

$$r(l') = r(l'T_s)$$
$$= \sum_{p=1}^{P} h_p e^{j2\pi \delta f_c \tau_p} \left(\frac{1}{\sqrt{M}} \sum_{n=0}^{N-1} \sum_{m=0}^{M-1} X(m, n) \right.$$
$$\left. g([l' - \frac{\tau_p}{T_s} - n(M+L)]T_s) e^{j2\pi m\Delta f([l' - \frac{\tau_p}{T_s} - n(M+L)]T_s)} \right)$$
$$e^{j2\pi(\delta f_c + \nu_p)(l'T_s - \tau_p)}, \quad (6)$$

where $l' \in \mathbb{Z}[0 \; N(M+L)]$. The n'th OTFS symbol with CP can be collected from the samples of received signal as $r(n'(M+L)+l), \forall l = 0, 1, \cdots, (M+L)-1$ and can be written as,

$$r(n'(M+L)+l)$$
$$= \sum_{p=1}^{P} h_p e^{j2\pi \delta f_c \tau_p}$$
$$(\frac{1}{\sqrt{M}} \sum_{n=0}^{N-1} \sum_{m=0}^{M-1} X(m, n) g([(n'-n)(M+L) + l - \frac{\tau_p}{T_s}]T_s)$$
$$e^{j2\pi m\Delta f([(n'-n)(M+L)]T_s)}$$
$$e^{j2\pi m\Delta f([l - \frac{\tau_p}{T_s}]T_s)} e^{j2\pi(\delta f_c + \nu_p)T_s(n'(M+L)+l - \frac{\tau_p}{T_s})} \quad (7)$$

We assume that, after initial coarse synchronization, a residual synchronization error of l_o samples from the starting index of CP removed OTFS symbol as shown in Fig.1 exists. We also assume $(l_0 T_s + \tau_{max}) \le T_{CP}$ so that no interference is experienced from the neighbouring OTFS symbols. The first step towards decoding the signal is to perform discrete Fourier Transform (DFT) on the CP removed samples of n'th OTFS symbol to obtain the time-frequency data and can be given as,
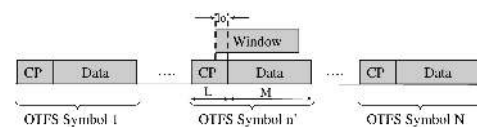

FIGURE 1. FFT Window Matching.

$$Y(m', n') = \frac{1}{\sqrt{M}} \sum_{k_t=0}^{M-1} r(n'(M+L) + L - l_0 + k_t) e^{-j\frac{2\pi m' k_t}{M}}. \tag{8}$$

Using (7) we can write,

$$Y(m', n')$$
$$= \frac{1}{M} \sum_{p=1}^{P} h_p e^{j2\pi \delta f_c \tau_p} e^{j2\pi(\nu_p + \delta f_c)T_s(L+n'(M+L)-l_o)}$$
$$e^{-j2\pi(\nu_p + \delta f_c)T_s(\frac{\tau_p}{T_s})} \sum_{n=0}^{N-1} \sum_{m=0}^{M-1} X(m, n)$$
$$e^{-j2\pi \frac{m(l_o + \frac{\tau_p}{T_s} + (n'-n)(M+L))}{M}}$$
$$\sum_{k_t=0}^{M-1} \left(g([(n'-n)(M+L) + L - l_o + k_t - \frac{\tau_p}{T_s}]T_s) \right.$$
$$\left. e^{-j2\pi \frac{k_t(m+(\nu_p+\delta f_c)T_s - m')}{M}} \right).$$

Since, $g(t)$ is a rectangular pulse,

$$g([(n'-n)(M+L) + L - l_0 + k_t - \frac{\tau_p}{T_s}]T_s)$$
$$= \begin{cases} 1, & \text{if } n = n' \ \& \ 0 \le (L - l_0 + k_t - \frac{\tau_p}{T_s})T_s \le T \\ 0, & \text{otherwise} \end{cases} \tag{9}$$

Then, (9) can be written as,

$$Y(m', n')$$
$$= \sum_{p=1}^{P} \tilde{h}_p e^{j2\pi \tilde{\nu}_p T_s(L+n'(M+L)-\frac{\tilde{\tau}_p}{T_s})}$$
$$\sum_{m=0}^{M-1} X(m, n') e^{-j2\pi \frac{m\tilde{\tau}_p}{MT_s}} \Psi((m + \tilde{\nu}_p T_s - m'), M), \tag{10}$$

where $\tilde{h}_p = h_p e^{j2\pi \delta f_c \tau_p}$, $\tilde{\nu}_p = (\nu_p + \delta f_c)$, $\tilde{\tau}_p = (\tau_p + l_0 T_s)$, $\Psi(x, M) \triangleq \frac{1}{M} \sum_{k_t=0}^{M-1} e^{-j\frac{2\pi k_t x}{M}}$. When $x \in \mathbb{Z}$, $\Psi(x, M) = \delta([x]_M)$. The time-frequency signal is transformed to delay-Doppler domain using symplectic finite Fourier transform (SFFT) as,

$$y(k', l') = \frac{1}{\sqrt{NM}} \sum_{n'=0}^{N-1} \sum_{m'=0}^{M-1} Y(m', n') e^{-j2\pi[\frac{n'k'}{N} - \frac{m'l'}{M}]}, \tag{11}$$

which can be simplified to (as shown in appendix C)

$$y(k', l')$$
$$= \sum_{p=1}^{P} \tilde{h}_p e^{j2\pi \tilde{\nu}_p T_s L} \sum_{k=0}^{N-1} \sum_{l=0}^{M-1} d(k, l)$$
$$\Psi(k - k' + \frac{\tilde{\nu}_p}{\Delta \nu}, N) \Psi(l - l' + \frac{\tilde{\tau}_p}{\Delta \tau}, M) e^{j2\pi \frac{\tilde{\nu}_p(l' - \frac{\tilde{\tau}_p}{\Delta \tau})}{\Delta \nu(M+L)N}}, \tag{12}$$

where $\Delta \nu = \frac{1}{(M+L)NT_s}$ and $\Delta \tau = T_s = \frac{1}{B}$ are Doppler and delay resolution at the receiver. Let $\tilde{\tau}_p = \tilde{l}_p \Delta \tau$ and $\tilde{\nu}_p = \tilde{k}_p \Delta \nu \implies \tilde{\nu}_p T_s = \frac{\tilde{k}_p}{(M+L)N}$, where $\tilde{l}_p, \tilde{k}_p \in \mathbb{R}$, then (12) can be written as,

$$y(k', l')$$
$$= \sum_{p=1}^{P} \left\{ \tilde{h}_p e^{j2\pi \frac{\tilde{k}_p L}{(M+L)N}} \sum_{k=0}^{N-1} \sum_{l=0}^{M-1} d(k, l) \right.$$
$$\left. \Psi(k - k' + \tilde{k}_p, N) \Psi(l - l' + \tilde{l}_p, M) e^{j2\pi \frac{\tilde{k}_p(l' - \tilde{l}_p)}{(M+L)N}} \right\} \tag{13}$$

III. EFFECTS OF RESIDUAL SYNCHRONIZATION ERRORS
In this section, we describe the effects of residual FTO and CFO errors in the receiver. From (12), it may be noted that $y(k', l')$ experiences ISI in both delay and Doppler dimension.

A. INTEGER DELAY AND INTEGER DOPPLER VALUES
When $\tilde{l}_p$ and $\tilde{k}_p$ are integers, then (12) simplifies as,

$$y(k', l') = \sum_{p=1}^{P} \left(h_p e^{j2\pi \delta f_c \tau_p} e^{j2\pi \nu'_p T_s L} \right.$$
$$\left. d(k' - k_p, l' - l_p) e^{j2\pi \frac{\nu'_p(l' - \frac{\tau'_l}{\Delta \tau})}{\Delta \nu'(M+L)N}} \right) \tag{14}$$

If we consider an AWGN scenario, then integer time and frequency errors result in a cyclic shift in delay and Doppler direction respectively thus cyclically shifting the origin of delay-Doppler grid to $(l_o, \frac{\delta f_c}{\Delta \nu})$. It can also be observed that, (14) resembles the received delay-Doppler signal as described in equation (24) of [3]. Thus the effect of synchronization error can be considered as a part of the channel itself, with modified channel taps $\tilde{h}_p = h_p e^{j2\pi \delta f_c \tau_p}$, $\tilde{\tau}_p = \tau_p + l_0 T_s$ & $\tilde{\nu}_p = \nu_p + \delta f_c$. Thus, it may be conjectured that channel equalization with appropriate channel coefficients may be able to equalize the effects of TVMC and residual synchronization errors.

B. INTEGER DELAY AND FRACTIONAL DOPPLER VALUES
By observing the the summation terms on the running variables l and k in (13) we can infer the following. If any Doppler or delay value of the modified channel is fractional, i.e. $\tilde{k}_p$ or $\tilde{l}_p \notin \mathbb{Z}$, then every symbol experiences interference in Doppler or delay dimension accordingly. The interference in the Doppler axis is observed frequently because the Doppler values of channel are not usually resolved to integer values. The residual synchronization error, δf_c, can lead to a modified fractional Doppler value even though the actual channel Doppler values (k_p) are integers since $\tilde{k}_p = k_p + \frac{\delta f_c}{\Delta \nu}$. Fractional delay values are not observed since the sampling of the received signal in time domain approximates the effect of fractional channel delay to the nearest integer time bin [3]. Thus $\tilde{l}_p \in \mathbb{Z} \implies (l - l' + \tilde{l}_p) \in \mathbb{Z} \ \forall \ l' \in [0 \ N-1] \implies \Psi(l - l' + \tilde{l}_p, M) = \delta([l - l' + \tilde{l}_p]_M)$. Therefore (13)

becomes,

$$y(k', l') = \sum_{p=1}^{P} \left\{ \tilde{h}_p e^{j2\pi \frac{\tilde{k}_p L}{(M+L)N}} \sum_{k=0}^{N-1} d(k, [l' - \tilde{l}_p]_M) \right.$$
$$\left. \Psi(k - k' + \tilde{k}_p, N) e^{j2\pi \frac{\tilde{k}_p (l' - \tilde{l}_p)}{(M+L)N}} \right\} \quad (15)$$

In (15), each received symbol experiences interference from all other symbols in Doppler dimension. In the sections that follow, we describe the construction of the equivalent channel matrix, its estimation and compensation of the effects of synchronization errors described here.

IV. EQUIVALENT CHANNEL MATRIX FOR OTFS INCLUDING SYNCHRONIZATION ERRORS

In this section, we derive the expression of equivalent channel matrix in time domain, which includes the effect of residual synchronization errors and time varying channel. For this, we establish the equivalent system model in matrix-vector form for CP-OTFS. Symbols $d(k, l)$ are arranged in $M \times N$ matrix as,

$$\mathbf{D} = \begin{bmatrix} d(0, 0) & d(1, 0) & \cdots & d(N-1, 0) \\ d(0, 1) & d(1, 1) & \cdots & d(N-1, 1) \\ \vdots & \vdots & \ddots & \vdots \\ d(0, M-1) & d(1, M-1) & \cdots & d(N-1, M-1) \end{bmatrix}.$$
$$(16)$$

Delay-Doppler to frequency-time domain conversion (after the ISFFT) is done following $\mathbf{X} = \mathbf{W}_M^\dagger \mathbf{D} \mathbf{W}_N$, where, $\mathbf{X} = \{X(m, n) \mid \forall m \in \mathbb{Z}[0 \ M-1] \& n \in \mathbb{Z}[0 \ N-1]\}$, such that frequency is along m and time is along n. Frequency-time domain to time domain signal is obtained using OFDM modulation, as $\mathbf{S} = \mathbf{W}_M \mathbf{X} = \mathbf{D} \mathbf{W}_N$, where $\mathbf{S} = [\mathbf{s}_0 \ \mathbf{s}_1 \ \cdots \ \mathbf{s}_{N-1}]$ is concatenation of OTFS symbol vectors $\mathbf{s}_i, \forall i \in [0 \ N-1]$. The pulse shaped samples of the signal is written as, $\mathbf{S}_{PS} = \mathbf{G}_T \mathbf{W}_M \mathbf{X}$. $\mathbf{G}_T$ is the pulse shaping matrix [25]. Since $g(t)$ is rectangular, we have $\mathbf{G}_T = \mathbf{I}_M$.

The CP appended signal is given as, $\mathbf{S}_{CP} = \mathbf{B}_{CP} \mathbf{S}_{PS} = \mathbf{B}_{CP} \mathbf{G}_T \mathbf{W}_M \mathbf{X} = \mathbf{B}_{CP} \mathbf{G}_T \mathbf{D} \mathbf{W}_N$, where $\mathbf{B}_{CP} = \begin{bmatrix} \mathbf{0}_{L \times M-L} & \mathbf{I}_L \\ & \mathbf{I}_M \end{bmatrix}$ is operator for appending CP. Thus, the transmit signal can be given as, $\mathbf{s}_{CP} = vec\{\mathbf{S}_{CP}\} = vec\{\mathbf{B}_{CP} \mathbf{G}_T \mathbf{D} \mathbf{W}_N\}$. Using the identity $vec\{\mathbf{A}_{K \times L} \mathbf{B}_{L \times M}\} = (\mathbf{I}_M \otimes \mathbf{A})vec\{\mathbf{B}\} = (\mathbf{B} \otimes \mathbf{I}_M)vec\{\mathbf{A}\}$, $\mathbf{s}_{CP} = (\mathbf{I}_N \otimes (\mathbf{B}_{CP} \mathbf{G}_T))vec\{\mathbf{D} \mathbf{W}_N\} = (\mathbf{I}_N \otimes \mathbf{B}_{CP})(\mathbf{W}_N^T \otimes \mathbf{I}_M)vec\{\mathbf{D}\} = (\mathbf{I}_N \otimes \mathbf{B}_{CP})(\mathbf{W}_N \otimes \mathbf{I}_M)\mathbf{d}$. Therefore,

$$\mathbf{s}_{CP} = \mathbf{A}_{CP}\mathbf{d}, \quad (17)$$

where $\mathbf{d} = vec\{\mathbf{D}\}$ is data vector, $\mathbf{A}_{CP} = (\mathbf{I}_N \otimes \mathbf{B}_{CP})\mathbf{A}$ and $\mathbf{A} = \mathbf{W}_N \otimes \mathbf{I}_M$. We also introduce the transmit signal vector $\mathbf{s} = vec\{\mathbf{S}\}$ without CP added and can be given as $\mathbf{s} = \mathbf{A}\mathbf{d}$ by putting $\mathbf{B}_{CP} = \mathbf{I}_M$ in (17). At the receiver, the noiseless

received signal in discrete form [3] can be written as,

$$\mathbf{r}_{CP}(l) = \sum_{p=1}^{P} h_p \mathbf{s}_{CP}(l - l_p) e^{j2\pi \frac{(l - l_p)k_p}{(M+L)N}}, \quad (18)$$

where $l \in \mathbb{Z}[0 \ ((M+L)N - 1)]$. We collect the samples $\mathbf{r}_{CP}(q(M+L) + l) \forall l \in \mathbb{Z}[0 \ M+L-1]$ to obtain qth OTFS symbol vector $\mathbf{r}_{CP}^q$ with CP. Then the CP removed vector $\mathbf{r}_q$ can be given as,

$$\mathbf{r}_q = \mathbf{R}_{CP}\mathbf{r}_{CP}^q, \quad \text{where } \mathbf{R}_{CP} = \begin{bmatrix} \mathbf{0}_{M \times L} & \mathbf{I}_M \end{bmatrix}. \quad (19)$$

Therefore,

$$\mathbf{r}_q(l) = \mathbf{r}_{CP}(q(M+L) + L + l), \ l \in [0 \ M-1]. \quad (20)$$

With the introduction of CFO at the receiver, the samples of qth received OTFS symbol $\mathbf{r}_q^f(l)$ is

$$\mathbf{r}_q^f(l) = \mathbf{r}_{CP}(q(M+L) + L + l) e^{j2\pi \frac{k_0(q(M+L) + L + l)}{N(M+L)}}, \quad (21)$$

where $k_0 = \frac{\delta f_c}{\Delta \nu}$. With residual time synchronization error of l_o samples,

$$\tilde{\mathbf{r}}_q(l) = \mathbf{r}_q^f(l - l_o)$$

From (18), (20) and (21),

$$\tilde{\mathbf{r}}_q(l)$$
$$= e^{j2\pi \frac{k_0(q(M+L) + L + l - l_o)}{N(M+L)}} \sum_{p=1}^{P} h_p e^{j2\pi \frac{k_p q}{N}}$$
$$e^{j2\pi \frac{(L + l - l_o - l_p)k_p}{(M+L)N}} \mathbf{s}_{CP}(q(M+L) + L + l - l_o - l_p). \quad (22)$$

We assume $l_o + l_\tau < L$. Therefore,

$$\tilde{\mathbf{r}}_q(l) = \sum_{p=1}^{P} h_p e^{j2\pi \frac{l_p k_0}{(M+L)N}} e^{j2\pi \frac{(k_p + k_0)q}{N}} e^{j2\pi \frac{(L + l - l_o - l_p)(k_p + k_0)}{(M+L)N}}$$
$$\mathbf{s}_q([l - l_p - l_o]_M). \quad (23)$$

Then,

$$\tilde{\mathbf{r}}_q = \begin{bmatrix} \tilde{\mathbf{r}}_q(0) \\ \tilde{\mathbf{r}}_q(1) \\ \vdots \\ \tilde{\mathbf{r}}_q(M-1) \end{bmatrix}$$
$$= \sum_{p=1}^{P} h_p e^{j2\pi \frac{l_p k_0}{(M+L)N}} \mathbf{\Pi}^{l_p + l_o} \mathbf{\Delta}^{k_p + k_0}$$
$$e^{j2\pi \frac{(k_p + k_0)(L - l_p - l_o)}{(M+L)N}} e^{j2\pi \frac{k_p + k_0}{N}q} \mathbf{s}_q, \quad (24)$$

where $\mathbf{\Pi} = circ\{[0 \ 1 \ 0 \cdots 0]_{M \times 1}^T\}$ is a circulant delay matrix and $\mathbf{\Delta} = \text{diag}\{[1 \ e^{j2\pi \frac{1}{(M+L)N}} \ \cdots e^{j2\pi \frac{M-1}{(M+L)N}}]^T\}$ is a diagonal Doppler matrix. Let, $\tilde{l}_p = l_p + l_o$, $\tilde{k}_p = k_p + k_0$ and $\tilde{h}_p = h_p e^{j2\pi \frac{l_p k_0}{(M+L)N}}$. When we include noise,

$$\tilde{\mathbf{r}}_q = \tilde{\mathbf{H}}_q \mathbf{s}_q + \mathbf{v}_q, \quad (25)$$

where $\mathbf{v}_q$ is M length Gaussian noise vector with elemental variance σ_v^2 and

$$\tilde{\mathbf{H}}_q = \sum_{p=1}^{P} \tilde{h}_p \mathbf{\Pi}^{\tilde{l}_p} \mathbf{\Delta}^{\tilde{k}_p} e^{j2\pi \frac{\tilde{k}_p(L-\tilde{l}_p)}{(M+L)N}} e^{j2\pi \frac{\tilde{k}_p}{N} q}. \quad (26)$$

The above can be modified as,

$$\tilde{\mathbf{H}}_q = \sum_{l=0}^{\tilde{l}_\tau} \mathbf{\Pi}^l \sum_{k \in \tilde{k}_{v_l}} diag\{\tilde{h_{l,k}} e^{j2\pi \frac{k(L-l)}{(M+L)N}}$$
$$e^{j2\pi \frac{k}{N} q} [1 \; e^{j2\pi \frac{k}{(M+L)N}} \; \cdots e^{j2\pi \frac{(M-1)k}{(M+L)N}}]^T\}, \quad (27)$$

where $\tilde{l}_\tau = l_\tau + l_0$ is maximum excess delay bin value of channel. We let k_{v_l} be the set of Doppler indices for the lth channel tap such that $P = \sum_{l=0}^{\tilde{l}_\tau} k_{v_l}$. Then $\tilde{k}_{v_l} = \{(k+k_0)| \; k \in k_{v_l}\}$ and

$$\tilde{h_{l,k}} = \begin{cases} \tilde{h}_p, & \text{if } \tilde{l}_p = l \text{ and } \tilde{k}_p = k \\ 0, & \text{otherwise.} \end{cases}$$

Therefore, the concatenation of CP removed vectors can be given as,

$$\tilde{\mathbf{r}} = \begin{bmatrix} \tilde{\mathbf{r}}_0 \\ \tilde{\mathbf{r}}_1 \\ \vdots \\ \tilde{\mathbf{r}}_{N-1} \end{bmatrix} = \underbrace{\begin{bmatrix} \tilde{\mathbf{H}}_0 & & & \\ & \tilde{\mathbf{H}}_1 & & \\ & & \ddots & \\ & & & \tilde{\mathbf{H}}_{N-1} \end{bmatrix}}_{\mathbf{H}} \underbrace{\begin{bmatrix} \mathbf{s}_0 \\ \mathbf{s}_1 \\ \vdots \\ \mathbf{s}_{N-1} \end{bmatrix}}_{\mathbf{s}} + \mathbf{v}, \quad (28)$$

which can be written as, $\tilde{\mathbf{r}} = \mathbf{Hs} + \mathbf{v} = \mathbf{HAd} + \mathbf{v}$, $\mathbf{v}$ being MN length concatenated white Gaussian noise vector. Equation (25) suggests that the effect of synchronization errors can be considered as part of time domain channel matrix. Equation (26) shows that the structure of the channel matrix is invariant to the introduction of synchronization errors which is an added advantage as the number of elements in the matrix does not change with residual synchronization errors and hence the sparsity of the matrix is unaltered. Next, we propose an estimation algorithm to estimate this equivalent channel matrix, however we first give a short justification for choooseing time domain channel estimation over delay-Doppler domain processing.

A. OTFS CHANNEL MATRICES

Delay-Doppler channel matrix $\mathbf{H}_{DD}$ and time domain channel matrix $\mathbf{H}$ are related as [25], $\mathbf{H}_{DD} = \mathbf{A}^\dagger \mathbf{HA}$. Using the definition of $\mathbf{A} = \mathbf{W}_N \otimes \mathbf{I}_M$, $\mathbf{H}_{DD}$ can be simplified as a block matrix with blocks of size $M \times M$ and can be written as, $\mathbf{H}_{DD} = \begin{bmatrix} \mathbf{H}_{dd}^{0,0} & \cdots & \mathbf{H}_{dd}^{(N-1),0} \\ \vdots & \ddots & \vdots \\ \mathbf{H}_{dd}^{0,(N-1)} & \cdots & \mathbf{H}_{dd}^{(N-1),(N-1)} \end{bmatrix}$, whose $(l, k)^{th}$ block can be given as, $\mathbf{H}_{dd}^{l,k} = \sum_{q=0}^{N-1} \bar{w}_{q,l} w_{q,k} \tilde{\mathbf{H}}_q$, where, $w_{l,k} = e^{j2\pi \frac{lk}{N}}$.

Finally, using the definition of $\tilde{\mathbf{H}}_q$ in (29), $\mathbf{H}_{dd}^{l,k}$ can be further simplified as,

$$\mathbf{H}_{dd}^{l,k} = \begin{cases} \sum_{p=1}^{P} \tilde{h}_p \mathbf{\Pi}^{\tilde{l}_p} \mathbf{\Delta}^{\tilde{k}_p} e^{j2\pi \frac{\tilde{k}_p(L-\tilde{l}_p)}{(M+L)N}} \delta([k - l + \tilde{k}_p]_N), \\ \quad \text{for } \tilde{k}_p \in \mathbb{Z} \\ \sum_{p=1}^{P} \tilde{h}_p \mathbf{\Pi}^{\tilde{l}_p} \mathbf{\Delta}^{\tilde{k}_p} e^{j2\pi \frac{\tilde{k}_p(L-\tilde{l}_p)}{(M+L)N}} \Psi(k - l + \tilde{k}_p, N), \\ \quad \text{for } \tilde{k}_p \notin \mathbb{Z} \end{cases}$$

We can infer the following from the above equation. When channel Doppler values are resolved in integer Doppler bins, each row of $\mathbf{H}_{DD}$ contains P matrices where $l - k = \tilde{k}_p$, $\forall p = 1, \cdots, P$ which results in NPN_e number of non-zero elements in $\mathbf{H}_{DD}$. However, when fractional Doppler is observed, the delay-Doppler channel matrix $\mathbf{H}_{DD}$ contains $N^2 N_e$ number of elements. Thus, structure of channel matrix varies with the nature of channel Doppler values which is not observed in time domain channel matrix. Therefore, $\mathbf{H}$ is at least P times and at max N times sparse than $\mathbf{H}_{DD}$. Therefore, equalization with $\mathbf{H}$ will result in lower complexity than equalization with $\mathbf{H}_{DD}$.

V. ESTIMATION OF EQUIVALENT CHANNEL MATRIX

In this section, we propose an algorithm to estimate the equivalent channel matrix specified in (27). From (27), we can write,

$$\tilde{\mathbf{H}}_q = \sum_{l=0}^{\tilde{l}_\tau} \mathbf{\Pi}^l \mathbf{H}_{q,l}, \text{ where,} \quad (29)$$
$$\mathbf{H}_{q,l} = diag\{[h(q(M+L)+L, l) \; h(q(M+L)+L+1, l)$$
$$\cdots h(q(M+L)+M+L-1, l)]^T\}, \quad (30)$$

where,

$$h(n, m) = \sum_{k \in \tilde{k}_{v_m}} h_{m,k} e^{j2\pi \frac{k_0 m}{N(M+L)}} e^{j2\pi \frac{k(n-m)}{N(M+L)}}, \quad (31)$$

$\forall \, n \in [0 \; N(M+L) - 1], m \in [0 \; \tilde{l}_\tau]$.

A. PILOT STRUCTURE IN DELAY-DOPPLER DOMAIN

We extend on the pilot structure described for OTFS in [14]. The pilot is a 2-dimensional (2D) impulse in delay-Doppler domain i.e. $d(k, l) = \sqrt{P_{PLT}} \delta(k - K_p, l - L_p)$, $\forall k \in [0 \; N - 1], l \in [L_p - L \; L_p + L - 1]$, where $P_{PLT} = N_p = 2NL$ is the pilot power. At the receiver, the received delay-Doppler signal corresponding to pilot signal, with synchronization error is,

$$y(k', l') = \sum_{p=1}^{P} \left\{ \tilde{h}_p e^{j2\pi \frac{\tilde{k}_p L}{(M+L)N}} \sum_{k=0}^{N-1} \sqrt{P_{PLT}} \delta(k - K_p, \right.$$
$$\left. [l' - L_p - \tilde{l}_p]_M) \Psi(k - k' + \tilde{k}_p, N) e^{j2\pi \frac{\tilde{k}_p(l'-\tilde{l}_p)}{(M+L)N}} \right\} \quad (32)$$

From the above, one may infer that the transmitted 2D impulse pilot, after going through the channel, spreads over the entire Doppler axis while the spread in delay is limited

to $(L_p + \tilde{l}_\tau)$ starting from L_p. We collect received signal $y(k', l')$, $\forall k \in [0 \ N - 1], l \in [L_p \ L_p + L - 1]$ for channel estimation. This part of the received signal contains the response of the channel to the 2D-delay-Doppler impulse pilot signal, which is not-interfered by data symbols. This is because we have assumed that $L \geq l_\tau + l_o - 1$.

B. CHANNEL ESTIMATION

Here we describe theorems necessary to obtain the time domain channel estimates from the received time domain signal. Theorem 1 relates the time domain channel coefficients and the received delay-Doppler signal $y(k', l')$. Theorem 2 establishes the relationship between the estimates of time domain channel coefficients and the received time domain signal $\mathbf{r}_{CP}(l)$.

Theorem 1: The intermittent time-domain channel coefficients are directly proportional to the N point IDFT values obtained from pilot section of received delay-Doppler grid, i.e, $h(\alpha(M+L)+L+L_p+l, l) = e^{-j2\pi \frac{\alpha K_p}{N}} \left(\sum_{k'=0}^{N-1} y(k', L_p + l) e^{j2\pi \frac{\alpha k'}{N}} \right)$, $\forall \ \alpha \in \mathbb{Z}[0 \ N - 1]$, $l \in \mathbb{Z}[0 \ \tilde{l}_\tau - 1]$.

Proof is given in Appendix A.

Theorem 2: The intermittent time-domain channel coefficients are directly proportional to the samples of received signal, i.e, $\hat{h}(\alpha(M + L) + L_p + l, l) = e^{-j2\pi \frac{\alpha K_p}{N}} \mathbf{r}_{CP}(\alpha(M + L) + L + L_p + l)$, $\alpha \in [0 \ N - 1]$

Proof is given in Appendix B.

From the above theorem, we see that the estimate of channel coefficients at time instances $(\alpha(M+L)+L_p+l)T_s$, $\alpha \in [0 \ N - 1]$ for lth channel tap can directly be obtained from $\mathbf{R}(l, k) = \mathbf{r}_k(l)$, as in Algorithm 1, without going through the FFT-ISFFT path to reach delay-Doppler domain as described in [14]. This creates the opportunity for estimating time domain channel coefficients from delay-Doppler domain embedded pilot. Using the estimated channel coefficients we obtain the values at time instances nT_s, $n \in \mathbb{Z}[0 \ N(M+L)-1]$ for each channel tap through interpolation. Since the coefficients to estimate (30) resembles a signal comprising sum of sinusoids, we considered the polynomial interpolation techniques (spline [26]) in this work. In other words,

$$
\begin{aligned}
h(n, l) = \text{spline\_interpolate}\Big(& [h(L_p + l, l) \\
& h(M + L + L_p + l, l) \\
& \cdots h((N - 1)(M + L) + L_p + l, l)]^T, \\
& \cdots [0 \ M + L(N - 1)(M + L)]^T, \\
& [0 \ 1 \ 2 \ \cdots \ (N)(M + L) - 1]^T \Big),
\end{aligned}
\tag{33}
$$

$\forall l \in [0 \ l_\tau - 1]$, where spline_interpolate (using 'interp1' inbuilt function in Matlab$^{\circledR}$), returns the interpolated signal at points u when y is the part of signal known at points x. Algorithm 1 describes how channel estimates for the entire time duration are generated from the received signal as well as how to estimate qth channel matrices $\hat{\mathbf{H}}_{q,i}$ & $\hat{\mathbf{H}}_q$, which are described in (30) & (29) respectively.

Algorithm 1 Estimation of $\tilde{\mathbf{H}}_q$

1: Given : The received signal $r(l)$
2: Output : $\hat{\tilde{\mathbf{H}}}_q$
3: $\mathbf{R}(l, k) = \mathbf{r}_k(l)$
4: **for** $l' = 0 : L$ **do**
5: $\quad \gamma = 0$
6: $\quad$ **for** $k = 0 : N - 1$ **do**
7: $\quad\quad \gamma = \gamma + \|\mathbf{R}(L_p + l', k)\|^2$
8: $\quad$ **end for**
9: $\quad$ **if** $\gamma > 3\sigma_n^2$ **then**
10: $\quad\quad l = [l \ l']$
11: $\quad\quad \hat{h}(n(M+L)+L+L_p+l', l') = \frac{1}{\sqrt{P_{PLT}}}\mathbf{R}(L_p+l', n)$
12: $\quad\quad \hat{h}(n, l') = \text{spline\_interpolate}(\{\hat{h}(n(M + L) + L + L_p+l', l') \mid n \in [0 \ N - 1]\}, [L+L_p+l' : M +L : N(M + L)], [0 : N(M + L) - 1])$
13: $\quad$ **end if**
14: **end for**
15: **for** $q = 0 : N - 1$ **do**
16: $\quad \hat{\mathbf{H}}_q = \mathbf{0}_{M \times M}$
17: $\quad$ **for** $i \in l$ **do**
18: $\quad\quad \hat{\mathbf{H}}_{q,i} = diag\{\{\hat{h}(q(M+L)+L+l', i)|l' \in [0 \ M-1]\}\}$
19: $\quad\quad \hat{\tilde{\mathbf{H}}}_q = \hat{\tilde{\mathbf{H}}}_q + \mathbf{\Pi}^i \hat{\mathbf{H}}_{l,\tau}^{q,i}$
20: $\quad$ **end for**
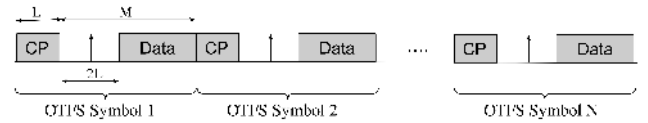21: **end for**

FIGURE 2. Time domain CP-OTFS frame.

C. TIME DOMAIN INTERPRETATION OF THE CHANNEL ESTIMATION

The frame structure used in delay-Doppler domain turns out to be a impulse train in the time domain modulated by sinusoid superimposed without interfering with the equivalent time domain data as shown in Fig.2 and is given as,

$$s(n) = s_p(n) + s_d(n). \tag{34}$$

Symbols $s_d(n)$ and $s_p(n)$ are the corresponding time domain equivalent signal of the the delay-Doppler data and pilot. Since pilot is a 2-D discrete impulse at location (K_p, L_p),

$$s_p(n) = \sqrt{\frac{P_{PLT}}{N}} e^{j2\pi \frac{K_p n}{N(M+L)}} \sum_{\alpha=0}^{N-1} \delta(n - (\alpha(M + L) + L + L_p)) \tag{35}$$

Using (18), (31), (34) and (35), the received signal is,

$$
\begin{aligned}
&r(n) \\
&= \sum_{l=0}^{l_\tau - 1} h(n, l)\Big(\sqrt{\frac{P_{PLT}}{N}} e^{j2\pi \frac{K_p(n-l)}{N(M+L)}} \sum_{\alpha=0}^{N-1}
\end{aligned}
$$

$$\delta(n - l - (\alpha(M + L) + L + L_p))) + \sum_{l=0}^{l_\tau - 1} h(n, l)s_d(n - l)$$

which can be simplified as,

$$r(n) = \sqrt{\frac{P_{PLT}}{N}} \sum_{\alpha=0}^{N-1} h(n, n - (\alpha(M + L) + L + L_p))$$
$$\times e^{j2\pi \frac{K_p(\alpha(M+L)+L+L_p)}{N(M+L)}} + \sum_{l=0}^{l_\tau - 1} h(n, l)s_d(n - l).$$

With length of CP being greater than τ_{max},

$$r(\alpha(M + L) + L + L_p + l) = \sqrt{\frac{P_{PLT}}{N}}$$
$$\times h(\alpha(M + L) + L_p + l, l)e^{j2\pi \frac{K_p(\alpha(M+L)+L+L_p)}{N(M+L)}}.$$

which implies that the result as obtained using theorem 2. From this time domain interpretation one can visualize the time domain frame as pilots embedded in each symbol. After such a pilot passes through a channel, one can obtain the channel impulse response directly. This can be interpolated to obtain the channel coefficients at all time instants as described earlier. In the next section we propose a low complexity LMMSE equalization technique, which uses the estimated equivalent channel matrix, to compensate for the channel induced distortions and residual synchronization errors.

VI. LMMSE EQUALIZATION

In this section, we explain a low complexity LMMSE receiver for CP-OTFS based on [15]. The LMMSE equalization of $\mathbf{r}$ in (28) results in estimated data vector $\hat{\mathbf{d}}$ given as,

$$\hat{\mathbf{d}} = (\mathbf{HA})^\dagger [(\mathbf{HA})(\mathbf{HA})^\dagger + \frac{\sigma_v^2}{\sigma_d^2}\mathbf{I}]^{-1}\mathbf{r}. \quad (36)$$

When $g(t)$ is rectangular, $\mathbf{A}$ becomes unitary. Thus (36) can be written as,

$$\hat{\mathbf{d}} = \mathbf{A}^\dagger \overbrace{\mathbf{H}^\dagger [\mathbf{HH}^\dagger + \frac{\sigma_v^2}{\sigma_d^2}\mathbf{I}]^{-1}\mathbf{r}}^{\mathbf{H}_{eq}}. \quad (37)$$
$$\underbrace{\qquad\qquad\qquad\qquad}_{\mathbf{r}_{ce}=\mathbf{H}_{eq}\mathbf{r}}$$

Thus LMMSE equalization can be performed as a two stage equalizer. In the first stage, LMMSE channel equalization is performed to obtain $\mathbf{r}_{ce} = \mathbf{H}_{eq}\mathbf{r}$. Second stage is a OTFS matched filter receiver to obtain $\hat{\mathbf{d}} = \mathbf{A}^\dagger\mathbf{r}_{ce}$. The direct implementation of $\mathbf{r}_{ce} = \mathbf{H}_{eq}\mathbf{r}$ requires inversion of $\Psi = \mathbf{HH}^\dagger + \frac{\sigma_v^2}{\sigma_d^2}\mathbf{I}$ and multiplication of $\mathbf{H}^\dagger$, which needs $O(M^3N^3)$ complex multiplications (CMs). Thus, it is desired to reduce the complexity of $\mathbf{r}_{ce} = \mathbf{H}_{eq}\mathbf{r}$. It is evident from (28), that $\mathbf{H}$ matrix is a block diagonal matrix with blocks $\tilde{\mathbf{H}}_q$ of size $M \times M$. This leads to $\Psi = \mathbf{HH}^\dagger + \frac{\sigma_v^2}{\sigma_d^2}\mathbf{I} = diag\{\Psi_0, \ \Psi_1, \ \cdots \ \Psi_{N-1}\}$, which is a block diagonal matrix

with blocks Ψ_q of size $M \times M$. It is well known that the inverse of a block diagonal matrix is also a block diagonal matrix. In addition to that, the inverse of a block diagonal matrix can be computed using the inverse of individual blocks. Similar to the decomposition of $\mathbf{r}$ into $\mathbf{r}_q$(s), $\mathbf{r}_{ce}$ can also be written as $\mathbf{r}_{ce} = [\mathbf{r}_{ce,0}^T \ \mathbf{r}_{ce,1}^T \cdots \mathbf{r}_{ce,N-1}^T]^T$, where $\mathbf{r}_{ce,q} = [\mathbf{r}_{ce}(q(M + L)+L) \ \mathbf{r}_{ce}(q(M+L)+L+1) \cdots \mathbf{r}_{ce}(q(M+L)+(M+L)-1)]^T$ is the qth, $q \in [0 \ N - 1]$ channel equalized vector. Thus we can write,

$$\mathbf{r}_{ce,q} = \tilde{\mathbf{H}}_q^\dagger [\tilde{\mathbf{H}}_q\tilde{\mathbf{H}}_q^\dagger + \frac{\sigma_v^2}{\sigma_d^2}\mathbf{I}]^{-1}\mathbf{r}_q, \ q \in \mathbb{Z}[0 \ N - 1], \quad (38)$$

which can be computed using inversion and multiplication of $M \times M$ matrices. The required complexity is of $O(NM^3)$. Generally, the value of M is in the order of 100's. Although the above simplifications significantly reduce complexity, yet LMMSE processing remains a computational burden. We investigate the structure of Ψ_q involved in channel equalization described earlier, in order to reduce the complexity further.

A. STRUCTURE OF $\Psi_Q = [\tilde{\mathbf{H}}_Q\tilde{\mathbf{H}}_Q^\dagger + \frac{\sigma_v^2}{\sigma_d^2}\mathbf{I}]$

Using (26), $\tilde{\mathbf{H}}_q\tilde{\mathbf{H}}_q^\dagger$ can be expressed as,

$$\tilde{\mathbf{H}}_q\tilde{\mathbf{H}}_q^\dagger$$
$$= \left(\sum_{p=1}^{P} \tilde{h}_p e^{j2\pi \frac{\tilde{k}_p(L-\tilde{l}_p)}{(M+L)N}} \boldsymbol{\Delta}^{\tilde{k}_p} \boldsymbol{\Pi}^{\tilde{l}_p} e^{j2\pi \frac{\tilde{k}_p}{N} q}\right)$$
$$\left(\sum_{s=1}^{P} \bar{\tilde{h}}_s e^{-j2\pi \frac{\tilde{k}_s(L-\tilde{l}_s)}{(M+L)N}} \boldsymbol{\Pi}^{-\tilde{l}_s} \boldsymbol{\Delta}^{-\tilde{k}_s} e^{j2\pi \frac{\tilde{k}_s}{N}(-q)}\right) \quad (39)$$

Since $\boldsymbol{\Pi}$ is a circulant matrix, it can be verified that $\boldsymbol{\Pi}^{l_p} = \mathbf{W}\boldsymbol{\Delta}^{-l_p}\mathbf{W}^\dagger$. Therefore, $\tilde{\mathbf{H}}_q\tilde{\mathbf{H}}_q^\dagger = \sum_{\substack{p=1 \\ p=s}}^{P} |\tilde{h}_p|^2\mathbf{I} + \sum_{\substack{p=1 \\ p\neq s}}^{P}\sum_{s=1}^{P} c_{p,s}\boldsymbol{\Pi}^{l_p-l_s}\boldsymbol{\Delta}^{k_p-k_s}e^{j2\pi q \frac{k_p-k_s}{N}}$, where $c_{p,s} = \tilde{h}_p\bar{\tilde{h}}_s e^{j2\pi \frac{-\tilde{k}_p\tilde{l}_p+\tilde{k}_s\tilde{l}_s}{(M+L)N}} e^{j2\pi \frac{L(\tilde{k}_p-\tilde{k}_s)}{(M+L)N}}$. Thus, we can write

$$\Psi_q = \sum_{\substack{p=1 \\ p=s}}^{P}(|\tilde{h}_p|^2 + \frac{\sigma_v^2}{\sigma_d^2})\mathbf{I} + \sum_{\substack{p=1 \\ p\neq s}}^{P}\sum_{s=1}^{P} c_{p,s}\boldsymbol{\Pi}^{\tilde{l}_p-\tilde{l}_s}\boldsymbol{\Delta}^{\tilde{k}_p-\tilde{k}_s}e^{j2\pi q \frac{\tilde{k}_p-\tilde{k}_s}{N}}. \quad (40)$$

From this, it can be concluded that the maximum shift of diagonal elements in $\boldsymbol{\Delta}$ can be $\pm(\tilde{l}_\tau - 1)$. Additionally, due to the cyclic nature of the shift, Ψ_q is quasi-banded with bandwidth of $2\tilde{l}_\tau - 1$. As $\tilde{l}_\tau \ll M$, Ψ_q is also sparse for typical wireless channel. Structure of Ψ_q is similar to the channel matrix of RCP OTFS as described in equation (13) specified in [15]. Thus Ψ_q^{-1} can be computed using LU factorization of Ψ_q in a similar way as described in Sec. III B of [15], i.e. $\Psi_q = \mathbf{L}_q\mathbf{U}_q$.

B. COMPUTATION OF $\hat{\mathbf{d}}$

After *LU* decomposition of Ψ_q, $\mathbf{r}_{ce,q}$ is simplified to,

$$\mathbf{r}_{ce,q} = \tilde{\mathbf{H}}_q^\dagger \overbrace{\mathbf{U}_q^{-1} \underbrace{\mathbf{L}_q^{-1} \mathbf{r}_q}_{\mathbf{r}_q^{(1)}}}^{\mathbf{r}_q^{(2)}}.$$

As $\mathbf{L}_q$ is a quasi-banded lower triangular matrix, $\mathbf{r}_q^{(1)} = \mathbf{L}_q^{-1}\mathbf{r}_q$ can be computed using low complexity forward substitution as explained in Algorithm 2 in [15]. Algorithm 3 of [15] can be used to evaluate $\mathbf{r}_q^{(2)} = \mathbf{U}_q^{-1}\mathbf{r}_q^{(1)}$. Using the definition of $\mathbf{H}_q$, $\mathbf{r}_{ce,q} = \tilde{\mathbf{H}}_q^\dagger \mathbf{r}_q^{(2)}$ can be written as,

$$\mathbf{r}_{ce,q} = \sum_{p=1}^P \bar{h}_p \boldsymbol{\Delta}^{-k_p} \underbrace{\boldsymbol{\Pi}^{-l_p}\mathbf{r}_q^{(2)}}_{\text{circular shift}}$$

. To compute $\mathbf{r}_{ce,q}$, $\mathbf{r}_q^{(2)}$ is first circularly shifted by '$-l_p$' and then multiplied by $\bar{h}_p \text{diag}\{\boldsymbol{\Delta}^{-k_p}\}$ using point-to-point multiplication for each path p. All vectors obtained above are summed to obtain $\mathbf{r}_{ce,q}$. Then, $\{\mathbf{r}_{ce,q}\}_{q=0}^{N-1}$ are concatenated to obtain $\mathbf{r}_{ce}$. Finally, $\hat{\mathbf{d}} = \mathbf{A}^\dagger \mathbf{r}_{ce}$ can be implemented using M number of N-point FFTs (Sec. III-C, [15]).

C. COMPUTATION COMPLEXITY

With some effort it can be shown that the number of CMs required to implement our proposed LMMSE algorithm is $\frac{MN}{2} \log_2 N + MN[2\, l_\tau^2 + 2\, P^2\, k_\nu + 9l_\tau - Pk_\nu - 3] + N[\frac{2}{3}l_\tau^3 + 2\, l_\tau + P]$. The order of complexity achieved through our receiver is $MN \log(MN)$, which is significantly lower than the direct implementation, which is of the order of M^3N^3. Our proposed receiver requires around 10^7x lower CMs than the direct implementation following (36), if we consider a typical OTFS system with $\Delta f = 15\, KHz$, $f_c = 4\, GHz$, $N = 128$, $M = 512$, speed of 500 kmph and the extended vehicular A (EVA) 3GPP channel model [27] with $P = 9$ and $\tau_{max} = 2.51\, \mu\, sec$.

It is worthwhile to note that we can also implement LMMSE receiver for OFDM [15] using the methods devised in the last section. The only difference between the receiver for OFDM and OTFS is the length of FFT used. For OTFS, we need M numbers of N-point FFTS whereas for OFDM we require N numbers of M-point FFTs. Thus, OTFS has complexity of O(MN $\log_2$(N))and OFDM has complexity of O(MN $\log_2$ (M)). In a typical OTFS settings, M > N, thus OFDM receiver has more computational burden than OTFS receiver.

VII. LDPC CODED LMMSE-SIC RECIEVER

We present the successive interference cancellation receiver for LDPC coded OTFS which uses the estimated channel coefficients instead of ideal channel coefficients [28]. In this description $\mathbf{r}_i^{int}$ contains the interfering signal for the ith iteration, where $1 \le i \le N_{SIC}$. The initial value is set as

$\mathbf{r}_1^{int} = 0$. In the ith iteration, interference is cancelled using,

$$\mathbf{r}_i = \mathbf{r} - \mathbf{r}_i^{int}. \tag{41}$$

It is required that $\mathbf{r}_i$ be equalized as,

$$\hat{\mathbf{d}}^{(i)} = \mathbf{A}^\dagger \mathbf{H}^\dagger [\mathbf{H}\mathbf{H}^\dagger + \frac{\sigma_v^2}{\sigma_d^2}\mathbf{I}]^{-1}\mathbf{r}_i. \tag{42}$$

Soft demapper output of $\hat{\mathbf{d}}^{(i)}$ are given to the LDPC [29] decoder to estimate the message bits $\hat{\boldsymbol{b}}_i$. The indices of correct blocks after i^{th} iteration are stored **indexc$^{(i)}$** with **indexc$^{(1)}$** $= 0$. Instead using the entire message, only the incorrectly decoded code blocks of the previous iteration are considered for decoding. The following is done accordingly $\hat{\mathbf{d}}^{(i)}[\mathbf{indexinc}] = \tilde{\tilde{\mathbf{d}}}^i$, where **indexinc** contains the indices of incorrect code words. The log-likelihood ratios(LLRs) of $\tilde{\tilde{\mathbf{d}}}^i$ are calculated as,

$$LLR(b_\eta^j|\tilde{\tilde{\mathbf{d}}}^i(\eta)) \approx (\min_{s \in S_j^0} \frac{||\tilde{\tilde{\mathbf{d}}}^i - s||^2}{\boldsymbol{\sigma}^2(\eta, \eta)}) - (\min_{s \in S_j^1} \frac{||\tilde{\tilde{\mathbf{d}}}^i - s||^2}{\boldsymbol{\sigma}^2(\eta, \eta)}) \tag{43}$$

where $\tilde{\tilde{\mathbf{d}}}^i(\eta)$ is the ηth element of $\tilde{\tilde{\mathbf{d}}}^i$ mapped from the bits $b_\eta^0\, b_\eta^1 \cdots b_\eta^{J-1}$, J is the number of bits per symbol and $\boldsymbol{\sigma}^2(\eta, \eta)$ is the element of $\boldsymbol{\sigma}^2 = \sigma_n^2(\mathbf{H}_{mmse}\mathbf{H}_{mmse}^\dagger)$, where $\mathbf{H}_{mmse} = \mathbf{A}^\dagger\mathbf{H}^\dagger[\mathbf{H}\mathbf{H}^\dagger + \frac{\sigma_v^2}{\sigma_d^2}\mathbf{I}]^{-1}$. S_j^0 and S_j^1 represent the constellation symbol sets where the bit $b_\eta^j = 0$ and $b_\eta^j = 1$ respectively for $j = 0, 1, \cdots, J - 1$. These LLRs are given as input to the LDPC decoder, which is based on the Min-Sum algorithm [30].

To generate the interference pattern $\mathbf{r}_{i+1}^{int}$, only the correctly decoded $\hat{\mathbf{d}}_i$ are used following,

$$\mathbf{r}_{i+1}^{int} = \mathbf{H}\mathbf{A}\tilde{\mathbf{d}}_i. \tag{44}$$

It may be noted that since we use correctly decoded code blocks for generation of interference pattern, error propagation is minimized unlike other SIC schemes which operates at uncoded symbol level.

Stopping Criteria: The SIC receiver is considered to iterate at most N_{SIC} times. Additional stopping criteria are with respect to improvement over iterations, i.e. iterations will stop if $\text{imp}_{fac} = N_e^i - N_e^{i-1} \le \eta_1$, where η_1 is improvement tolerance constant and N_e^i is the number of blocks in error after i^{th} iteration. We also stop the SIC iterations if $\text{err}_{fac} = N_e^i \le \eta_2$, where η_2 is error threshold value, i.e. number of error blocks are very low already.

VIII. UNIFIED FRAMEWORK FOR ORTHOGONAL MULTICARRIER SYSTEMS

In this section, we describe a generalized framework for orthogonal waveforms. Modulation techniques following this framework will be able to take advantage of the channel estimation and equalization algorithms proposed earlier. Let $\mathbf{D}$ be the data matrix of size $(M) \times N$. Then the transmit signal which can be of the form

$$\mathbf{S}_d = \{\mathfrak{B}\mathbf{D}\mathfrak{C}\} = \mathbf{A}vec\{\mathbf{D}\}, \tag{45}$$
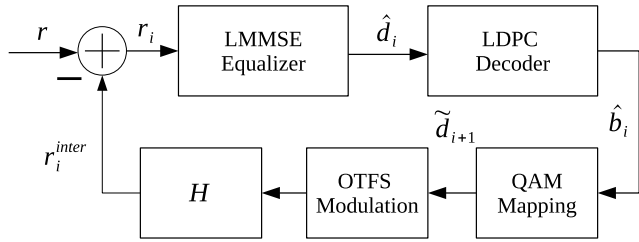
FIGURE 3. Schematic block diagram representing signal flow of our proposed code word level SIC receiver.

Algorithm 2 SIC Receiver

1: Given : $\mathbf{r}$, $\mathbf{H}$, η_1 and η_2
2: Output : $\hat{\boldsymbol{b}}$
3: Initialize : $imp_{fac} = 10\eta_1$ $err_{fac} = 10\eta_2$, $\mathbf{indexc^1} = 0$
4: $\mathbf{r}_1^{int} = \mathbf{0}$ and $\tilde{\mathbf{d}}_1 = \mathbf{0}$
5: Compute $\Psi = [\mathbf{HH}^\dagger + \frac{\sigma_v^2}{\sigma_d^2}\mathbf{I}]$
6: Compute $\mathbf{LU} = \Psi$
7: **while** ($i \leq N_{SIC}$ && $imp_{fac} \geq \eta_1$ && $err_{fac} \geq \eta_2$) **do**
8:     $\mathbf{r}_i = \mathbf{r} - \mathbf{r}_i^{int}$
9:     $\hat{\mathbf{d}}^{(i)} = \mathbf{A}^\dagger \mathbf{H}^\dagger \mathbf{U}^{-1} \mathbf{L}^{-1} \mathbf{r}_i$
10:     $\hat{\mathbf{d}}^{(i)}[\mathbf{indexinc^{(i)}}] = \tilde{\mathbf{d}}^i$
11:     $[\hat{\boldsymbol{b}}_i, \mathbf{indexinc}^{(i)}] = LDPCdecoder (\tilde{\hat{\mathbf{d}}}^{(i)})$
12:     $\tilde{\mathbf{d}}_{i+1} = QAMmod (\hat{\boldsymbol{b}}_i)$
13:     $\tilde{\mathbf{d}}_{i+1}[\mathbf{index_inc}^{(i)}] = 0$
14:     $\mathbf{r}_{i+1}^{int} = \mathbf{HA}\tilde{\mathbf{d}}_{i+1}$
15:     $imp_{fac} = N_e^i - N_e^{i-1}$
16:     $err_{fac} = N_e^i$
17: **end while**
18: $\hat{\boldsymbol{b}} = \hat{\boldsymbol{b}}_{N_{SIC}}$

---

where $\mathfrak{B}$ and $\mathfrak{C}$ are modulation specific matrices. $\mathbf{A}$ in (36) can be computed using $\mathbf{A} = (\mathfrak{C} \otimes \mathbf{I})(\mathbf{I} \otimes \mathfrak{B})$. We define $\mathbf{S}_p$ as the constant pilot matrix of size $2L \times N$ as

$$\mathbf{S}_p = \begin{bmatrix} \mathbf{0}_{L \times N} \\ [1 \ 1 \ \cdots 1]_{1 \times N} \\ \mathbf{0}_{L-1 \times N} \end{bmatrix}. \quad (46)$$

The combined time domain matrix with N symbols each containing M samples can be given as, $\mathbf{S} = \begin{bmatrix} \mathbf{S}_p \\ \mathbf{S}_d \end{bmatrix}$. We append CP as described before, i.e. $\mathbf{S}_{CP} = \mathbf{B}_{CP}\mathbf{S}$. Then, the transmit vector can be given as $\mathbf{s} = vec\{\mathbf{S}_{CP}\}$. This transmit vector will resemble the time domain frame illustrated in Fig. 2. Hence, the same time domain channel estimation and low complexity LMMSE equalization proposed can be used to equalize the combined effects of channel and residual synchronization errors.

CP-OTFS presented in this work can be fitted in this framework when one sets $\mathfrak{B} = \mathbf{I}_M$ and $\mathfrak{C} = \mathbf{W}_N$ in above equations. Similarly, when $\mathfrak{B} = \mathbf{W}_M$ and $\mathfrak{C} = \mathbf{I}_N$, the above system becomes an OFDM system with no difference in the equalization techniques at the receiver. Hence, this generalized description of system can pave the way to realize

a flexible communication system which can change its waveform with changing nature of channel, for e.g., the transceiver pair can use OFDM in low mobility scenarios while switching to OTFS under high speed scenario.

IX. RESULTS

In this section, we present the performance of low density parity check (LDPC) coded CP-OTFS system with time domain channel estimation and equalization in presence of residual FTO and CFO errors. Since we present a unified model for constructing OFDM signal as well as OTFS signal, therefore we also present the performance of an equivalent OFDM system. We also present the performance of the developed time domain channel estimation when used with RCP-OFTS, however without residual synchronization errors. The simulation parameters used are mentioned in Table 1. For each channel delay tap value, Doppler is generated using Jake's formula, $v_p = v_{max} cos(\theta_p)$, where θ_p is uniformly distributed over $[-\pi \ \pi]$. CP length is chosen longer than τ_{max} of the TVMC.

TABLE 1. Simulation parameters.

Parameter	Value
Carrier Frequency(f_c)	6 GHz
Bandwidth(B)	7.68 MHz
Frame Time(T_f)	8.7 ms
Subcarrier Bandwidth(Δf)	15 KHz
OTFS parameters	M=512, N=128 , $\Delta\nu = 117.18$ Hz, $\Delta\tau = 130.21$ ns
Pilot location	$K_p=0$, $L_p=10$
Channel Model	EVA [27]
CP duration	$T_{CP} = 1.302 \ \mu s$, $L = 10$
UE speed	500 kmph
Modulation	16-QAM
FEC (LDPC)	Coderate $\frac{2}{3}$, Codeword Length 648

The curves labeled 'Ideal' represent the performance of LMMSE equalization with ideal channel estimate without any residual synchronization error. The legend 'mmse' indicates the performance of LMMSE equalizer while using estimated channel coefceints, similary 'sic' indicates performance of SIC receiver with estimated channel coefficients. The numeral following these key words indicates the number of Doppler taps per delay tap ('Dpt') used in evaluation. The legend 'synch' indicates situations where $l_0 = 2$ and $k_0 = 20$. In case of 'synch' estimated channel coefficients are used in LMMSE equalization and 'sic'. Normalized CFO error $k_0 = \frac{\delta f_c}{\Delta \nu} = 20$ results in $\delta f_c = k_0 \Delta \nu = 2.33$ KHz.

A. BLOCK ERROR RATE (BLER) PERFORMANCE

We begin with the BLER performance of CP-OTFS system using Figure 4. Let us first consider the 'Ideal' performance. It is observed that as 'Dpt' increases, the performance of

the system improves. At BLER of 10^{-1}, the difference in performance is nearly 4 dB. At BLER of 10^{-2}, the SNR gain is approximately 6 dB. At higher reliability the gain increases further. This gain in performance with increasing value of Dpt can be attributed to Doppler diversity. This diversity is due to increase in the number of independent channel paths with increasing value of Dpt. It also indicates that the LMMSE receiver is able to extract this diversity from the received signal.
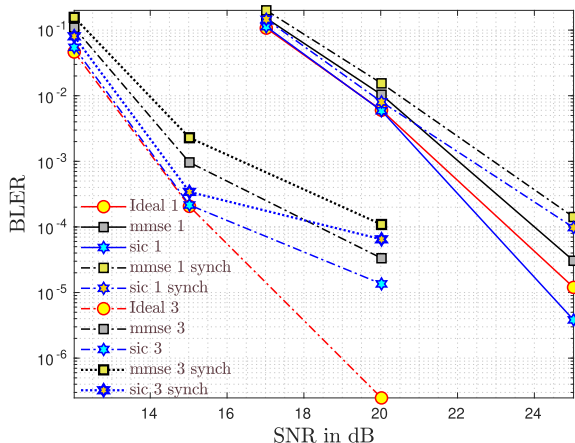

FIGURE 4. BLER Vs SNR (dB) for CP-OTFS with 16-QAM, ldpc code word length 648, code rate $= \frac{2}{3}$ at 500 kmph.

Next, we consider the performance of CP-OTFS with the proposed channel estimation algorithm but without residual synchronization error. The degradation in performance in 'mmse' from 'Ideal' is limited to approximately 1 dB for all considered Dpt. Whereas for 'sic' the performance loss from 'Ideal' is negligible.

Now we turn our attention to the performance of CP-OTFS system with synchronization errors (legend marked with 'synch') while using the estimation and compensation techniques described above. In case of 'mmse', it can be seen that for 1 Dpt, the degradation in performance when compared to no synchronizatin error is nearly 0.5 dB, which is about 1.5 dB for 3 Dpt. Whereas, in case of 'sic' it may be noted that the performance is not much deviated from 'Ideal' untill error floor starts to appear at higher SNRs. It may also be noted that CP-OTFS is fully immune to residual synchronization error.

After having discussed the performance of CP-OTFS with 16-QAM, which captures the impact of phase modulation as well as amplitude modulation we include the performance of the proposed algorithms for a higher order QAM, namely 64-QAM. The BLER vs SNR of 64-QAM is presented in Fig. 5. It can be seen that at a BLER of 10^{-1}, the additional SNR required, over 16-QAM, is about 7 dB. Whereas, it is around 10 dB at BLER of 10^{-3} and below. A very interesting observation that can be made for higher order QAM is that the SIC performance improves significantly over single stage MMSE. Such results are supported in [28], [31].
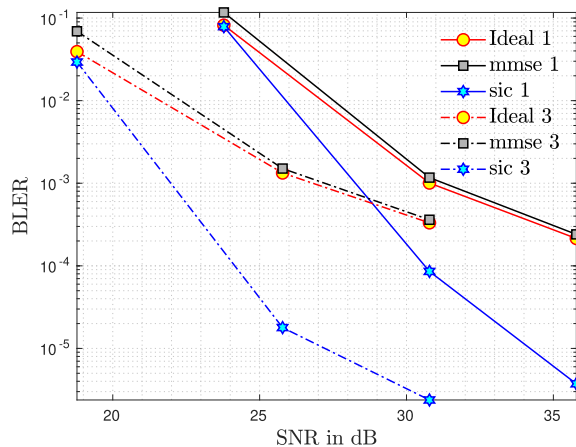

FIGURE 5. BLER Vs SNR for 64-QAM with ldpc code word length 648, code rate $= \frac{2}{3}$ at 500 kmph.

From the above it can be said that the proposed channel estimation algorithm along with the SIC receiver can be highly recommended for CP-OTFS systems.

We present additional results related to larger code block length, lower mobility and lower code rate in Appendix D for the sake of completeness.

Considering that RCP-OTFS is more spectrally efficient than CP-OTFS, we intend to examine the performance of the proposed time domain channel estimation for RCP-OTFS as well through Fig. 6. We have extending the above desribed algorithms for RCP-OTFS by cosidering the CP length to be zero for all except the first CP, which is drawn from the entire OTFS block. Due to brevity we do not provide the details which are all but similar to what has been described in the above sections however without effects of residual synchronization errors. Since RCP-OTFS with residual synchronization errors require development of dedicated algorithims, which is beyond the scope of this work, we present results with only channel estimation without residual synchronization errors.
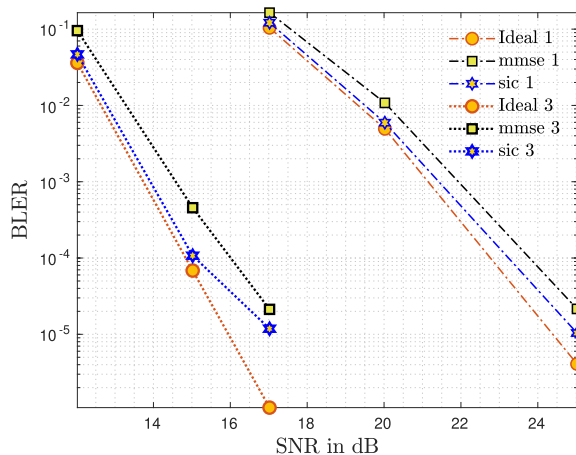

FIGURE 6. BLER Vs SNR (dB) for RCP-OTFS with 16-QAM, ldpc code word length 648, code rate $= \frac{2}{3}$ at 500 kmph.

Upto BLER of 10^{-2} we can see there is not much difference in performance between CP-OTFS and RCP-OTFS. Although RCP-OTFS is expected to encounter a large amount of interference owing to lack of CP between the OFDM symbols, however the pilot structure as explained above helps to reduce inter-OFDM-symbol interference. At higher SNR RCP-OTFS is found to perform slightly better than CP-OTFS. This can be attributed to improved channel estimation owing to higher rate of pilot sampling due to lesser time interval between the pilot sample points. It is also noted that with 3 Doppler taps per delay tap the performance of RCP-OTFS is slightly better than CP-OTFS. The most significant point to be noted here is that the developed channel estimation can be translated to RCP-OTFS, however without 'synch' errors.

Now we present the performance of OFDM system, which is described in Section VIII, in Fig. 7. The very first observation one can make is that SIC does not provide any notable improvement in performance. The reason being that in OFDM systems, the QAM symbols are carried on each sub-carrier whereas in OTFS they are spread over the entire time-frequency space. Another quick observation reveals that with Dpt of 3, the performance is better by nearly 5 dB over the scenario of 1 Dpt. Now let us compare OFDM against CP-OTFS. We first consider that 'Ideal, 'mmse' and 'sic' cases without residual synchronization errors. When Dpt 1 scenario is taken, we find that OFDM is poorer by nearly 3 dB at BLER of 10^{-1}. The gap increases to nearly 5 dB at BLER of 10^{-2} and it continues to increase further as SNR increases. This clearly indicates the superiority of OTFS over OFDM by virtue of its diversity gain. If we consider the case of 3 Dpt, we again find that at low SNR, CP-OTFS is better than OFDM by nearly 3 dB. The difference is about 7 dB at BLER of 10^{-2}, again indicating higher diversity gain obtained by OTFS over OFDM. When we turn our attention to the 'synch' cases, we find that OFDM is severly limited, which is not a new finding. In comparison we find the CP-OTFS has significant resilience to such large residual synchronization error although not completely immune to it.

From the above discussions, it can be said that the proposed algorithms can provide sufficient resilience to OTFS against synchronization errors while compensating for TVMC and thus makes OTFS a potential transmission technology candidate for use especially in high mobility scenarios.

Having exposed the most important performance metrics of OTFS under TVMC and residual synchronization errors, we now take a look at the mean square error (MSE) of the channel estimates for the strongest tap against varying SNR for different Dpt as shown in Fig. 8. It can be observed that the MSE increases with Dpt. Thus, one can infer that the channel coefficients obtained from the interpolation based channel estimation deviate from actual channel coefficients as Dpt increases. Although MSE for Dpt of 3 is worse than that for Dpt of 1, the BLER performance of Dpt 3 is better. This can be attributed to the improved diversity experienced
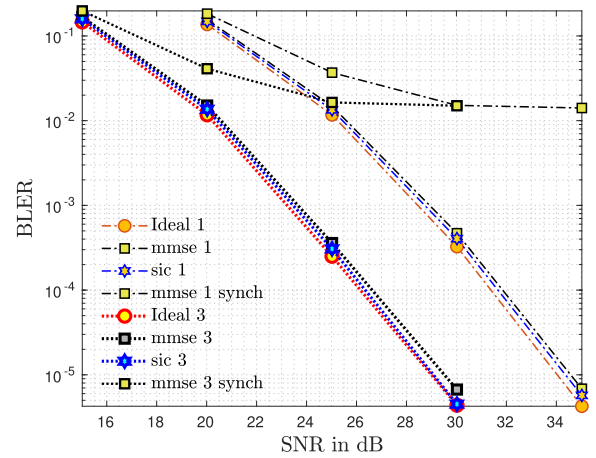

FIGURE 7. BLER Vs SNR for CP-OFDM with 16-QAM, ldpc code word length 648, code rate $= \frac{2}{3}$ at 500 kmph.

due larger number of independent paths available. Further, the MSE values are small enough so as not to affect the performance significantly. One of the reasons is that the pilot being an impulse in delay-Doppler as well as in time domain enjoys significantly higher SNR than the data part of the signal.
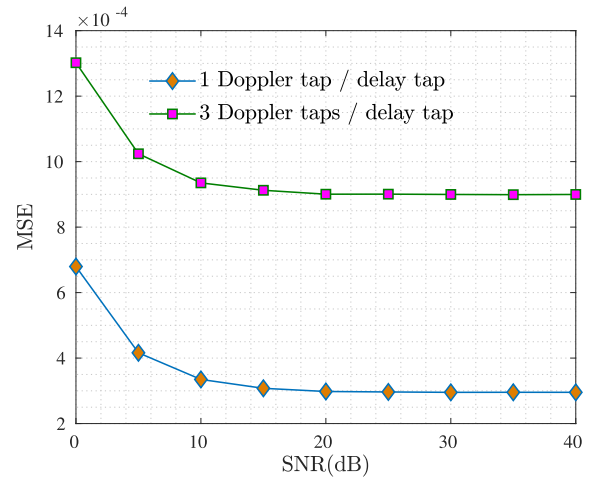

FIGURE 8. MSE of channel estimates for CP-OTFS.

It can also be observed that MSE saturates even when SNR increases. This indicates that the proposed estimation and compensation methods are effective only in the mid-SNR region. One may wonder that the saturation in MSE should be observed in the BLER curves as well. This is indeed true, however, the saturation in BLER starts to appear below the level of 10^{-3}.

B. LIMIT OF CFO TOLERANCE

Since we are concerned about the effect of residual synchronization errors, of which the CFO has more significant effect on the received signal, we present the BLER performance of CP-OTFS against normalized CFO ($\frac{\delta f_c}{\Delta \nu}$) in Fig.9. For Dpt
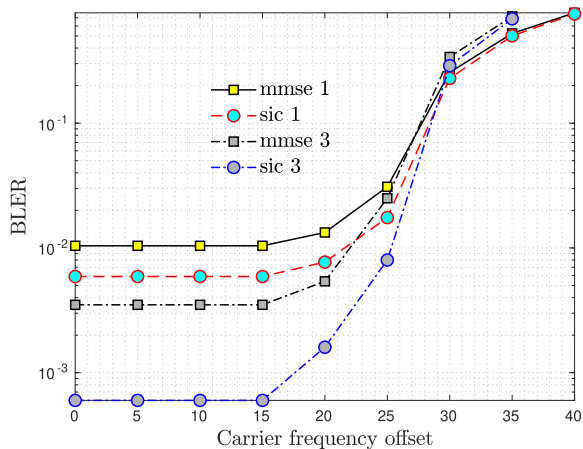
FIGURE 9. BLER Vs Normalized CFO for CP-OTFS with 16-QAM, ldpc code word length 648, code rate = $\frac{2}{3}$ at 500 kmph.
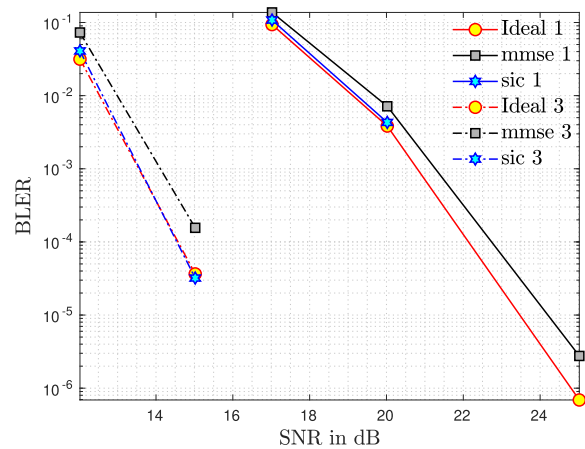

FIGURE 10. MSE of channel estimates with varying CFO.

FIGURE 11. BLER Vs SNR for 16-QAM with ldpc code word length 648, code rate = $\frac{1}{2}$ at 500 kmph.

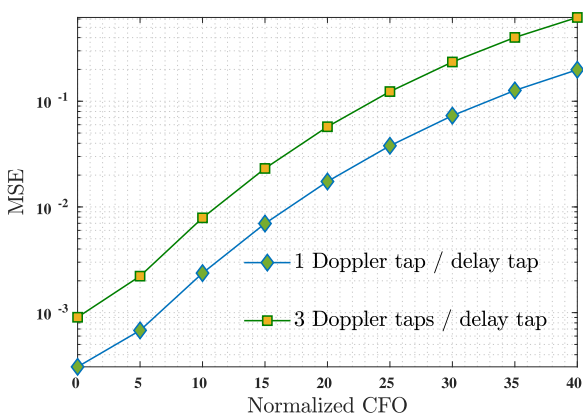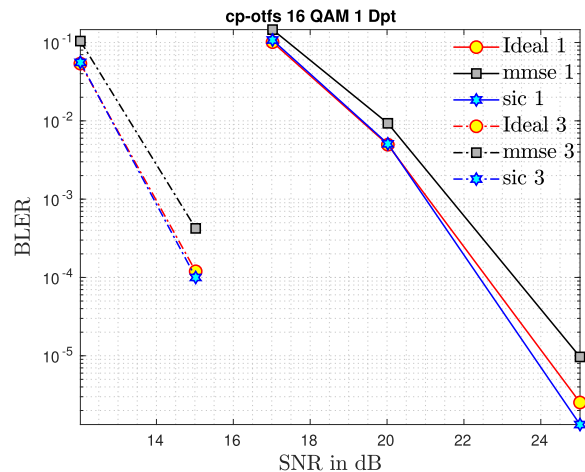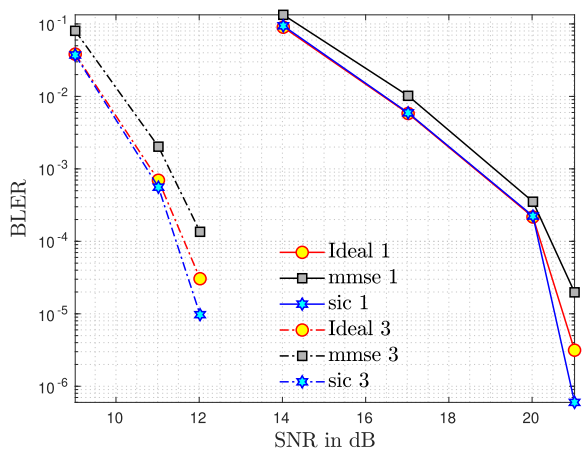**FIGURE 12.** BLER Vs SNR for 16-QAM with ldpc code word length 1944, code rate = $\frac{2}{3}$ at 500 kmph.

FIGURE 13. BLER Vs SNR for 16-QAM with ldpc code word length 648, code rate = $\frac{2}{3}$ at 100 kmph.

The increase in MSE is due to an increasing mismatch between the estimates of channel coefficients obtained using the proposed method and the actual value of channel coefficients. An increase in CFO, which has a similar effect as increase in Doppler, results in a higher rate of channel fluctuations. An increase in the frequency of time-domain pilots may help in improving the situation but it has its associated penalty in terms of spectral efficiency loss, the detailed analysis of which is beyond the scope of this work.

Therefore it may be said that, with a limited allowable SNR degradation from the ideal performance, our proposed channel estimation method can compensate normalized CFO value up to 20. However, it may also be stated that beyond such values the performance of CP-OTFS degrades at significantly. A normalized CFO value of 20 leads to an offset value of $\delta f_c = 20\Delta \nu = 2.33 \ kHz$ which is 15% of the sub-carrier bandwidth and is 0.4 ppm of carrier frequency. This value can be considered as a significantly high limit of residual frequency error, which can be addressed by the methods described in this work. It is important to mention that the performance is evaluated considering channel conditions

of 1, we consider SNR of 20 dB, whereas for Dpt of 3, we use SNR of 14 dB.

It can be observed that BLER does not increase notably untill normalized CFO reaches a value of 20, beyond which it grows exponentially. This increase in BLER can be attributed to increase in MSE with CFO observed in Fig.10, which shows the MSE of channel estimates for the strongest tap.

where the maximum Doppler frequency is 2.76kHz, which is additive in nature with CFO as discussed in Section III. This results in a significantly high value of equivalent maximum Doppler of 5.09 kHz.

X. CONCLUSION

We have started by describing the system model of a rectangular pulse shaped CP-OTFS system with residual frame timing offset and residual carrier frequency offset errors. We exposed that integer time and frequency errors result in a cyclic shift in delay and Doppler dimensions. We also show that fractional Doppler or delay causes interference in Doppler or delay dimension respectively. Since we found that the effect of synchronization errors can be considered as a part of the channel itself, however with modified channel taps, we developed a time domain channel estimation method for delay Doppler domain embedded pilot based CP-OTFS system to estimate the effective channel matrix. It is brought out that the time domain processing offers lower complexity owing to higher sparsity compared the delay Doppler domain channel under the presence of residual synchronization errors.

Using the estimates of the effective channel matrix, we presented a low complexity LMMSE receiver as well as a SIC based receiver for LDPC coded CP-OTFS system. It is seen that CP-OTFS has significantly large tolerance to residual CFO, however it is not completely immune to it. It is found that the maximum SNR loss at BLER 10^{-2} is around 1 dB in the absence of residual synchronization errors when LMMSE is used, however the loss is negligible when SIC is used. It is also shown that the described compensation methods show promise to compensate for residual CFO of up to 15% of subcarrier bandwidth or 0.4 ppm of carrier frequency with a loss in SNR up to 1.5 dB at BLER 10^{-2} in case of LMMSE. However it is found that SIC can bring the performance close to LMMSE with ideal channel estimates. It is also seen that iterative SIC gives massive gains especially for higher order QAM modulations. We have verified that the presented channel estimation and compensation methods can be translated to RCP-OTFS as well. We have shown that OTFS with practical channel estimation in presence of residual synchronization errors significantly outperforms OFDM (by 3 - 7 dB) especially when such errors are high as encountered in high ICI conditions. With the above, it can be stated that the proposed time domain channel estimation and LMMSE based SIC receiver for LDPC coded CP-OTFS can enable OTFS for use as potential air interface in high mobility conditions.

Considering that OFDM with frequency-domain adaptive modulation and coding is known for providing high spectral efficiency especially in low mobility conditions and that OTFS provides much superior reliability in high mobility conditions, the unified framework for representing both modulations depicted in this work can help pave the path for a flexible and reconfigurable future air interface.

APPENDIX A
PROOF OF THEOREM 1

Proof: $y(k', L_p + l') = \sum_{l=0}^{\tilde{l}_\tau} \delta(l' - l) \sum_{k \in k_{v_i}} \Big\{ \tilde{h}_{l,k} \Psi(K_p - k' + k_p, N) e^{j2\pi \frac{k_p(L+l'+L_p-l)}{(M+L)N}} \Big\}$. At lth tap, i.e when $l = l'$, $y(k', L_p + l) = \sum_{k \in k_{v_l}} \Big\{ \tilde{h}_{l,k} e^{j2\pi \frac{k(L_p+L)}{(M+L)N}} \Psi(K_p - k' + k, N) \Big\}$.

When IFFT of (M+L)N point is applied and it can be shown that,

$$\sum_{k'=0}^{N-1} y(k', L_p + l) e^{j2\pi \frac{nk'}{N(M+L)}}$$

$$= \sum_{k \in k_{v_l}} \Big\{ \tilde{h}_{l,k} e^{j2\pi \frac{k(L_p+L)}{(M+L)N}} \Big(\frac{1}{N} \sum_{k_t=0}^{N-1} e^{j2\pi \frac{k_t(K_p+k)}{N}} \sum_{k'=0}^{N-1} e^{j2\pi \frac{k'(n-k_t(M+L))}{N(M+L)}} \Big) \Big\}$$

$$= \begin{cases} \sum_{k \in k_{v_l}} \Big\{ \tilde{h}_{l,k} e^{j2\pi \frac{k(L_p+L)}{(M+L)N}} (e^{j2\pi \frac{n(K_p+k)}{N(M+L)}}) \Big\}, & n = \alpha(M + L) \\ \sum_{k_t=0}^{N-1} e^{j2\pi \frac{k_t(K_p)}{N}} \Psi((\frac{n}{(M+L)} - k_t), N) \sum_{k \in k_{v_l}} \\ \Big\{ \tilde{h}_{l,k} e^{j2\pi \frac{k(L_p+L)}{(M+L)N}} \Big\} e^{j2\pi \frac{k_t(k)}{N}}, & otherwise. \end{cases}$$

From (31), $h(n, m) =$

$$\begin{cases} h(n + L_p + L + l, l) e^{j2\pi \frac{n(K_p)}{N(M+L)}}, & n = \alpha(M + L) \\ \sum_{k_t=0}^{N-1} e^{j2\pi \frac{k_t(K_p)}{N}} \Psi((\frac{n}{(M+L)} - k_t), N) \\ h(k_t(M + L) + L_p + L + l, l), & otherwise. \end{cases}$$

Hence, $h(\alpha(M + L) + L + L_p + l, l) =$

$$e^{-j2\pi \frac{\alpha K_p}{N}} \Big(\sum_{k'=0}^{N-1} y(k', L_p + l) e^{j2\pi \frac{\alpha k'}{N}} \Big)$$

$\square$

APPENDIX B
PROOF OF THEOREM 2

Proof: We know, $\hat{h}(\alpha(M + L) + L_p + l, l) = e^{-j2\pi \frac{\alpha K_p}{N}} \Big(\sum_{k'=0}^{N-1} y(k', L_p + l) e^{j2\pi \frac{\alpha k'}{N}} \Big)$. Also, as explained in the [10], the time domain signal can be viewed as the interleaved OFDM, in which an N-point FFT is taken along the Doppler axis and then interleaved to get the time domain signal. If this is applied to the received delay-Doppler signal $y(k', l')$, then the signal without CP can be given as, $r(\alpha(M) + l') = \Big(\sum_{k'=0}^{N-1} y(k', l') e^{j2\pi \frac{\alpha k'}{N}} \Big)$. Due to addition of CP, $r(\alpha(M + L) + L + l') = \Big(\sum_{k'=0}^{N-1} y(k', l') e^{j2\pi \frac{\alpha k'}{N}} \Big)$. Therefore, $\hat{h}(\alpha(M+L) + L_p + l, l) = e^{-j2\pi \frac{\alpha K_p}{N}} r(\alpha(M + L) + L + L_p + l)$.

$\square$

APPENDIX C
PROOF:DELAY-DOPPLER INPUT-OUTPUT RELATION

$$y(k', l') = \frac{1}{\sqrt{NM}} \sum_{n'=0}^{N-1} \sum_{m'=0}^{M-1} Y(n', m') e^{-j2\pi [\frac{n'k'}{N} - \frac{m'l'}{M}]}$$

Using (1) and (10), with some effort it can be simplified as,

$$
\begin{aligned}
y(k', l') = \frac{1}{NM} \sum_{p=1}^{P} \tilde{h}_p e^{j2\pi \tilde{v}_p T_s (L - \frac{\tilde{\tau}_p}{T_s})} \\
\sum_{k=0}^{N-1} \sum_{l=0}^{M-1} d(k,l) \sum_{m=0}^{M-1} \sum_{m'=0}^{M-1} e^{-j2\pi \frac{m\tilde{\tau}_p}{MT_s}} e^{j2\pi \frac{m'l'}{MT_s}} \quad (47) \\
\Psi(m + \tilde{v}_p T_s - m', M) \\
\sum_{n'=0}^{N-1} e^{j2\pi \frac{n'(\tilde{v}_p T_s N(M+L) + k - k')}{N}}. \text{ By substituting,}
\end{aligned}
$$

$\Psi(m + \tilde{v}_p T_s - m', M) = \frac{1}{M} \sum_{k_t=0}^{M-1} e^{-j2\pi \frac{k_t(m + \tilde{v}_p T_s - m')}{M}}$, we can write,

$$
\begin{aligned}
y(k', l') \\
= \frac{1}{NM^2} \sum_{p=1}^{P} \tilde{h}_p e^{j2\pi \tilde{v}_p T_s (L - \frac{\tilde{\tau}_p}{T_s})} \\
\sum_{k=0}^{N-1} \sum_{l=0}^{M-1} d(k,l) \left(\sum_{n'=0}^{N-1} e^{j2\pi \frac{n'(\tilde{v}_p T_s N(M+L) + k - k')}{N}} \right) \quad (48) \\
\sum_{k_t=0}^{M-1} e^{-j2\pi k_t (\tilde{v}_p T_s)} \sum_{m=0}^{M-1} e^{-j2\pi \frac{m}{M}(k_t - l - \frac{\tilde{\tau}_p}{T_s})} \sum_{m'=0}^{M-1} e^{j2\pi \frac{m'(l'-k_t)}{M}}
\end{aligned}
$$

Since $(l' - k_t) \in \mathbb{Z}$, we substitute $e^{j2\pi \frac{m'(l'-k_t)}{M}} = M\delta[(l' - k_t)_M]$, $\frac{1}{N} \sum_{n'=0}^{N-1} e^{j2\pi \frac{n'(\tilde{v}_p T_s N(M+L) + k - k')}{N}} = \Psi(\tilde{v}_p T_s N(M+L) + k - k', N)$ and $\frac{1}{M} \sum_{m=0}^{M-1} e^{-j2\pi \frac{m}{M}(k_t - l - \frac{\tilde{\tau}_p}{T_s})} = \Psi(k_t - l - \frac{\tilde{\tau}_p}{T_s}, M)$, therefore we get,

$$
\begin{aligned}
y(k', l') = \frac{1}{M} \sum_{p=1}^{P} \tilde{h}_p e^{j2\pi \tilde{v}_p T_s (L - \frac{\tilde{\tau}_p}{T_s})} \sum_{k=0}^{N-1} \sum_{l=0}^{M-1} d(k,l) \\
\Psi(\tilde{v}_p T_s N(M+L) + k - k', N) \sum_{k_t=0}^{M-1} e^{-j2\pi k_t (\tilde{v}_p T_s)} \\
\Psi(k_t - l - \frac{\tilde{\tau}_p}{T_s}, M) \left(M\delta[(l' - k_t)_M] \right). \quad (49)
\end{aligned}
$$

Using $\Delta\tau = \frac{1}{B} = T_s \; \Delta v = \frac{1}{N(M+L)T_s}$ and $l' = k_t$,

$$
\begin{aligned}
y(k', l') \\
= \sum_{p=1}^{P} \tilde{h}_p e^{j2\pi \tilde{v}_p T_s (L)} \sum_{k=0}^{N-1} \sum_{l=0}^{M-1} d(k,l) \Psi(\frac{\tilde{v}_p}{\Delta v} \\
+ k - k', N) \Psi(l + \frac{\tilde{\tau}_p}{\Delta\tau} - l', M) e^{-j2\pi(l' - \frac{\tilde{\tau}_p}{\Delta\tau})(\frac{\tilde{v}_p}{\Delta v N(M+L)})}
\end{aligned}
$$

APPENDIX D
ADDITIONAL RESULTS

In this section we present additional results pertaining to the effect of lower code rate, larger code word length, and lower mobility conditions on 16-QAM based CP-OTFS system. We begin with the performance of rate code $\frac{1}{2}$ in Fig. 11. We compare it against the result shown in Fig. 4, which is for code rate $\frac{2}{3}$. At a BLER of 10^{-1}, it can be observed that code rate $\frac{1}{2}$ provides approximately 3 dB improvement over code rate $\frac{2}{3}$. A gain of around 4 dB is found at lower BLER values.

The effect of larger code block length is shown in Fig. 12. By comparing against Fig. 4 it can be seen that at BLER of 10^{-1} there is only little gain, however the gain is around 1 dB near BLER of 10^{-3} and it increases further at lower BLER values. Thus the gain with higher code block length is observed with more intensity at lower BLER / higher SNR regions.

The performance at lower mobility, i.e., at 100 kmph is shown in Fig. 13. Again we take Fig. 4 as reference for comparison. It can be observed that there is no note worthy difference. Such observation is also reported in [3].

REFERENCES

[1] *IMT Traffic Estimates for the Years 2020 to 2030*, ITU, Geneva, Switzerland, 2015.

[2] (Nov. 2017). *Minimum Requirements Related to Technical Performance for IMT-2020 Radio Interface(s)*. [Online]. Available: https://www.itu.int/pub/R-REP-M.2410-2017

[3] P. Raviteja, K. T. Phan, Y. Hong, and E. Viterbo, "Interference cancellation and iterative detection for orthogonal time frequency space modulation," *IEEE Trans. Wireless Commun.*, vol. 17, no. 10, pp. 6501–6515, Oct. 2018.

[4] F. Hlawatsch, *Wireless Communications Over Rapidly Time-Varying Channels*, 1st ed. Oxford, U.K.: Academic, 2011.

[5] *NR Physical Channels and Modulation (Release 15)*, documentTS 38.211, V 15.2, 3GPP, 2018.

[6] S. S. Das, E. D. Carvalho, and R. Prasad, "Performance Analysis of OFDM Systems with Adaptive Sub Carrier Bandwidth," *IEEE Trans. Wireless Commun.*, vol. 7, no. 4, pp. 1117–1122, Apr. 2008.

[7] S. S. Das, "Variable guard interval orthogonal frequency division multiplexing in presence of carrier frequency offset," in *Proc. IEEE Global Telecommun. Conf*, vol. 5, Oct. 2005, p. 2941.

[8] S. S. Das, "Techniques to enhance spectral efficiency of OFDM wireless systems," Ph.D. dissertation, Dept. Electron. Syst. (ES), Aalborg Univ., Aalborg, Denmark, 2007.

[9] (Nov. 2019). *Detailed Specifications of the Terrestrial Radio Interfaces of International Mobile Telecommunications-Advanced (IMT-Advanced)*. [Online]. Available: https://www.itu.int/rec/R-REC-M.2012/en

[10] V. Rangamgari, "OTFS: Interleaved OFDM with block CP," in *Proc. Nat. Conf. Commun. (NCC)*, vol. 2020, pp. 1–6.

[11] F. Wiffen, "Comparison of OTFS and OFDM in ray launched sub-6 GHz and mmWave line-of-sight mobility channels," in *Proc. IEEE 29th Annu. Int. Symp. Pers. Indoor Mobile Radio Commun.*, Sep. 2018, pp. 73–79.

[12] P. Raviteja, E. Viterbo, and Y. Hong, "OTFS performance on static multipath channels," *IEEE Wireless Commun. Lett.*, vol. 8, no. 3, pp. 745–748, Jun. 2019.

[13] R. Hadani, "Orthogonal Time Frequency Space Modulation," in *Proc. IEEE WCNC*, Mar. 2017, pp. 1–6.

[14] P. Raviteja, K. T. Phan, Y. Hong, and E. Viterbo, "Embedded delay-Doppler channel estimation for orthogonal time frequency space modulation," in *Proc. IEEE 88th Veh. Technol. Conf. (VTC-Fall)*, Aug. 2018, pp. 1–5.

[15] S. Tiwari, S. S. Das, and V. Rangamgari, "Low complexity LMMSE receiver for OTFS," *IEEE Commun. Lett.*, vol. 23, no. 12, pp. 2205–2209, Dec. 2019.

[16] G. D. Surabhi and A. Chockalingam, "Low-complexity linear equalization for OTFS modulation," *IEEE Commun. Lett.*, vol. 24, no. 2, pp. 330–334, Feb. 2020.

[17] K. R. Murali and A. Chockalingam, "On OTFS modulation for high-Doppler fading channels," in *Proc. Inf. Theory Appl. Workshop (ITA)*, Feb. 2018, pp. 1–10.

[18] P. Raviteja, K. T. Phan, Q. Jin, Y. Hong, and E. Viterbo, "Low-complexity iterative detection for orthogonal time frequency space modulation," in *Proc. IEEE Wireless Commun. Netw. Conf. (WCNC)*, Apr. 2018, pp. 1–6.

[19] M. K. Ramachandran, G. D. Surabhi, and A. Chockalingam, "OTFS: A new modulation scheme for high-mobility use cases," *J. Indian Inst. Sci.*, vol. 100, no. 2, pp. 315–336, Apr. 2020, doi: 10.1007/s41745-020-00167-4.

[20] W. Yuan, Z. Wei, J. Yuan, and D. W. K. Ng, "A simple variational Bayes detector for orthogonal time frequency space (OTFS) modulation," *IEEE Trans. Veh. Technol.*, vol. 69, no. 7, pp. 7976–7980, Jul. 2020.

[21] W. Shen, L. Dai, J. An, P. Fan, and R. W. Heath, Jr., "Channel estimation for orthogonal time frequency space (OTFS) massive MIMO," *IEEE Trans. Signal Process.*, vol. 67, no. 16, pp. 4204–4217, Aug. 2019.

[22] Y. Hebron, S. S. Rakib, R. Hadani, and M. Tsatsanis, "Channel acquisition using orthogonal time frequency space modulated pilot signal," U.S. Patent 10 749 651 B2, Aug. 18, 2020.

[23] K. Witrisal, "OFDM air interface design for multimedia communications," Ph.D. dissertation, Delft Univ. Technol., Delft, The Netherlands, 2002.

[24] R. Hadani, S. Rakib, A. F. Molisch, C. Ibars, A. Monk, M. Tsatsanis, J. Delfeld, A. Goldsmith, and R. Calderbank, "Orthogonal time frequency space (OTFS) modulation for millimeter-wave communications systems," in *IEEE MTT-S Int. Microw. Symp. Dig.*, Jun. 2017, pp. 681–683.

[25] P. Raviteja, Y. Hong, E. Viterbo, and E. Biglieri, "Practical pulse-shaping waveforms for reduced-cyclic-prefix OTFS," *IEEE Trans. Veh. Technol.*, vol. 68, no. 1, pp. 957–961, Jan. 2019.

[26] J. C. Bartels, *Hermite and Cubic Spline Interpolation Ch. 3 in An Introduction to Splines for Use in Computer Graphics and Geometric Modelling*. 1998.

[27] *Guidelines for Evaluation of Radio Interface Technologies for IMT-Advanced*, ITU, Geneva, Switzerland, 2009.

[28] S. S. Das, "Performance of iterative successive interference cancellation receiver for LDPC coded OTFS," in *Proc. IEEE Int. Conf. Adv. Netw. Telecommun. Syst.*, Dec. 2020, pp. 1–5

[29] *Ieee Standard for Information Technology—Local and Metropolitan Area Networks—Specific Requirements—Part 11: Wireless Lan Medium Access Control (MAC) and Physical Layer (PHY) Specifications Amendment 5: En- Hancements for Higher Throughput*, Standard 802.11n-2009, 2009.

[30] J. Zhao, "On implementation of min-sum algorithm and its modifications for decoding low-density parity-check (LDPC) codes," *IEEE Trans. Commun.*, vol. 53, no. 4, pp. 549–554, Apr. 2005.

[31] R. Hadani, "Orthogonal time frequency space modulation," 2018, *arXiv:1808.00519*. [Online]. Available: https://arxiv.org/abs/1808.00519

VIVEK RANGAMGARI received the B.Tech./M.Tech. degree from the Department of Electronics and Electrical Communication Engineering, IIT Kharagpur, India, in 2020. He has been actively working in the physical layer signal processing for wireless communication since 2018.

SHASHANK TIWARI (Member, IEEE) received the M.Tech. degree in telecommunication system engineering from IIT Kharagpur, Kharagpur, India, in 2011, where he is currently pursuing the Ph.D. degree with the G. S. Sanyal School of Telecommunication. He has served as a Faculty Member with The LNM Institute of Information Technology, Jaipur, India, from 2011 to 2013. His current research interests include wireless communications, digital signal processing for communications, and 5G waveform design.

SUVRA SEKHAR DAS (Member, IEEE) received the B.Eng. degree in electronics and communication engineering from the Birla Institute of Technology, Ranchi, India, and the Ph.D. degree from Aalborg University, Aalborg, Denmark. He was the Senior Scientist of the Innovation Laboratory, Tata Consultancy Services. He is currently an Associate Professor with the G. S. Sanyal School of Telecommunications, IIT Kharagpur, Kharagpur, India. His current research interests include design of waveform, radio access technology, and radio access networks for QoS traffic.

SUBHAS CHANDRA MONDAL (Senior Member, IEEE) received the degree in electronics and electrical communications engineering from IIT Kharagpur. He is currently a Wipro Fellow and the Chief Architect of the organization-wide 5G initiative at Wipro. He has more than 27 years engineering experience in Telecom Research and Development. He is a passionate Technologist and has developed several solutions and frameworks in emerging technology areas, such as 5G, SDN/NFV, Li-Fi, cyber security, and AI for network automation. Prior to Wipro, he has worked for C-DOT as a Research Engineer and developed a remote switching product ground-up.

• • •